



# The Tectonic Map and Structural Provinces of the Late Neoproterozoic Egyptian Nubian Shield: Implications for Crustal Growth of the Arabian–Nubian Shield (East African Orogen)

Zakaria Hamimi<sup>1,2</sup>, Wael Hagag<sup>1</sup>, Harald Fritz<sup>3</sup>, Haitham Baggazi<sup>4</sup> and Samir Kamh<sup>5\*</sup>

<sup>1</sup>Geology Department, Faculty of Science, Benha University, Benha, Egypt, <sup>2</sup>Department of Geological Sciences, Faculty of Science, Galala University, New Galala City, Egypt, <sup>3</sup>Department of Earth Sciences, University of Graz, Graz, Austria, <sup>4</sup>Structural Geology and Remote Sensing Department, Faculty of Earth Sciences, King Abdulaziz University, Jeddah, Saudi Arabia, <sup>5</sup>Geology Department, Faculty of Science, Tanta University, Tanta, Egypt

## OPEN ACCESS

### Edited by:

Ahmed M. Eldosouky,  
Suez University, Egypt

### Reviewed by:

Mohamed Abdelkareem,  
South Valley University, Egypt  
Islam Abou El-Magd,  
National Authority for Remote Sensing  
and Space Sciences, Egypt  
Nivaldo Destro,  
Petrobras, Brazil

### \*Correspondence:

Samir Kamh  
skamh@science.tanta.edu.eg

### Specialty section:

This article was submitted to  
Structural Geology and Tectonics,  
a section of the journal  
Frontiers in Earth Science

**Received:** 16 April 2022

**Accepted:** 13 May 2022

**Published:** 30 June 2022

### Citation:

Hamimi Z, Hagag W, Fritz H, Baggazi H  
and Kamh S (2022) The Tectonic Map  
and Structural Provinces of the Late  
Neoproterozoic Egyptian Nubian  
Shield: Implications for Crustal Growth  
of the Arabian–Nubian Shield (East  
African Orogen).  
Front. Earth Sci. 10:921521.  
doi: 10.3389/feart.2022.921521

The Late Neoproterozoic Egyptian Nubian Shield (ENS) has attracted increasing attention since the establishment of the Egyptian Geological Survey and Mining Authority (EGSMA (1896)), which conducted the first mapping. In the last three decades, rapid improvements in analytical techniques, along with field-oriented studies, have made it possible for the interpretation of the ENS as an integral part of the juvenile Arabian–Nubian Shield (ANS) as a portion of the East African Orogen (EAO). However, a consistent tectonic map of the ENS does not exist. Presentation of such a map is the main objective of the present work where Landsat-based lithological discrimination is combined with the systematic structural investigation and careful reassessment of previously published geological maps. Our interpretation of this map indicates that in accordance with previous work, the basement units of the Eastern Desert (ED) can be divided into three structural domains: Northern, Central, and South-Eastern Desert provinces. The proposed provinces are ascribed to three different plate tectonic far-field boundary conditions. The earliest magmatic, metamorphic, and tectonic history was set off by the approximate north–south convergence of the Gabgaba–Gebeit, Jiddah–Asir terranes, and Eastern Desert–Midyan terranes along the Yanbo–Onib–Sol–Hamid–Gerf–Allaqi–Heiani (YOSHGAH) suture between c. 800 and 620 Ma. The second event between c. 640 and 580 Ma was correlated with the Nabitah Orogeny when the Ad Dawadimi–Ar Rayn terranes in the eastern Arabian Shield accreted to the earlier consolidated arc terranes (Afif and Tathlith terranes). During this period, east–west convergence between northwestern Saudi Arabia and the Central Eastern Desert (CED) in Egypt caused a pronounced strike-slip deformation associated with the displacement along the wider Najd Fault system. The third orogenic phase, which was younger than c. 580 Ma, was controlled by the evolution and retreat of the Cadomian Arc. The northern portions of the ENS and the northern

Arabian Shield experienced extension whereas extensive post-orogenic magmatism was related to mantle delamination and associated crustal thinning.

**Keywords:** Egyptian Nubian Shield, tectonic map, structural provinces, far-field stresses, flow fields, remote sensing

## INTRODUCTION

The Late Neoproterozoic Egyptian Nubian Shield (ENS), which includes the Eastern Desert (ED) and Sinai, is a contiguous part of the Arabian–Nubian Shield (ANS), a northern continuation of the East African Orogen (EAO) (**Figure 1**). The ANS was formed by the accretion of island arc tectonic terranes sutured along megashear zones decorated by ophiolites. The late orogenic evolution was characterized by transcurrent plate motion that developed a complex pattern of post-accretionary strike-slip and extensional shear zones. The Eastern Desert (ED) is one of these tectonic terranes that demonstrated a conspicuous window of the Neoproterozoic tectonic, magmatic, and metamorphic evolution of the ANS. The Late Neoproterozoic belt of the ED was dominated by ophiolitic nappes, arc-related volcano-sedimentary sequences, and post-amalgamation molasse sediments, which all were accompanied by emplacement of various magmatic suites. From the tectonic perspective, the ED was subdivided into exhumed high-grade metamorphosed gneiss domes (“infrastructure”) mantled by lower-grade metamorphosed volcano-sedimentary suites (“suprastructure”). The tectonically and magmatically related exhumation of gneissic domes was associated with the deposition of post-amalgamation molasse sediments. The rock classification and tectonic evolution of the Egyptian basement in ED were strongly premised on the infrastructural-suprastructural orogenic model (Akaad and Noweir, 1980; El-Gaby et al., 1988; Abdel Khalek et al., 1992; Khudeir and Asran, 1992). Ophiolitic nappes, arc-related metavolcanics, and volcanoclastic–metasediments constituted the suprastructural rocks (or “Tier-2” of Bennet and Mosley, 1987). These rocks were thrust during the Neoproterozoic on the gneisses–migmatites and their remobilized equivalents that represented the infrastructural rocks (or Tier-1 of Bennet and Mosley, 1987; Abdel Khalek et al., 1992). Such a two-tier model suggested a sub-horizontal and penetrating sole thrust (infrastructure–suprastructure transition and ED decollement of Stern, 2017) that separated the lower and upper ED crustal layers.

Remarkable differences in the lithology and structural architecture of the exposed ED basement led Stern and Hedge (1985) and El-Gaby et al. (1988) to subdivide ED into three tectonic provinces: North Eastern Desert (NED), Central Eastern Desert (CED), and South Eastern Desert (SED) (**Figure 2A**). The NED province comprises voluminous granitic intrusions with some exposures of island arc metavolcanics, metasediments, and Hammamat Molasse sediments. In contrast, the CED province is dominated by arc metavolcanics, metasediments, and ophiolitic nappes, which were associated with some gneissic domal structures delineated by transcurrent shear zones (Fritz et al., 1996; Bregar et al., 2002). The SED province is generally composed of complex areas of migmatitic gneisses, foliated

granodiorites, and high-grade schistose-metasediments (El-Gaby et al., 1988; Hermina et al., 1989). These provinces were believed to be juxtaposed along major shear zones. The Qena-Safaga shear zone separated the NED from CED, and the Idfu-Mersa Alam shear zone separated the CED from SED. Furthermore, the northerly dipping Nugrus-Shait shear zone was considered to be the tectonic boundary between CED and SED (Fowler and Osman, 2009). One of the objectives of the present study is to expand this model and explain the lithological and structural differences using the differences in the plate motions of the involved plates.

The infracrustal-supracrustal orogenic model and tripartite classification of the ED have been generally agreed upon by the scientific community for decades. However, the studies remained descriptive with little potential for clarifying the causes. Structural, tectonic, and isotopic data have newly been released in the form of comprehensive reviews focused on the tectonic evolution of the ED (Greiling et al., 1994; Johnson et al., 2011; Fritz et al., 2013; Stern, 2017; Hamimi et al., 2019; Hamimi and Abd El-Wahed, 2020; El-Kalioubi et al., 2020; Fowler and Hamimi, 2020; Stern and Ali, 2020). In addition, modern plate tectonic reconstructions (Collins et al., 2021a; Collins et al., b) provide a far-field tectonic framework for EAO that inspired questions on the credibility of these old basement models and classifications. In the present study we develop a new tectonic map of ENS that incorporates these new studies. The main objective of the present work is the development of such a tectonic map based on intensive field/structural work and processing and analysis of the images of optical sensors by remote sensing techniques (15 Landsat-8 OLI/TIRS images, **Figure 2B**). We also reexamine and upgrade the previous maps published by EGSMA, CONOCO, and other research works and projects. ENS is a typical example of well-exposed crystalline basement rocks suitable to apply Landsat-8 data for geological and structural mapping. The structural succession and distribution of the characteristic rock assemblages extracted from this map are further used to establish a tectonic model of the ED. The differences in structural associations within the different ED domains are explained and the differences in the plate motions of involved plates (“far-field stress”) and partitioned deformation along major high strain zones (“local response”).

## TECTONOSTRATIGRAPHY OF THE ENS

The ENS includes a vast tract of igneous and metamorphic rock complexes (about 100,000 km<sup>2</sup>) exposed along the Red Sea Hills in the ED and occupies a triangular area in Southern Sinai (**Figures 2A, B**). It lies in the northwestern part of the ANS and is composed mainly of a juvenile continental crust of the Neoproterozoic age. The Egyptian basement complex comprises

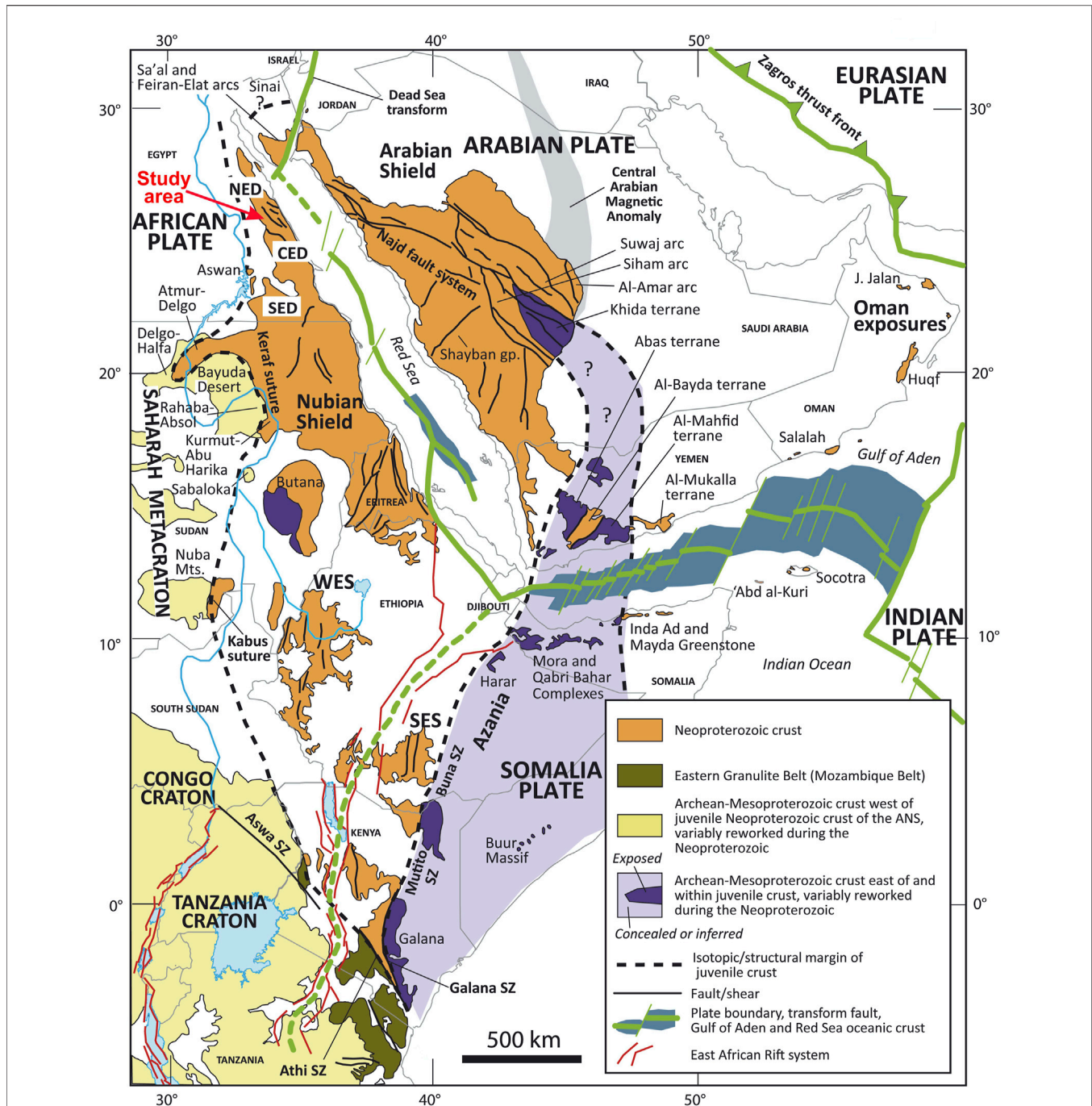
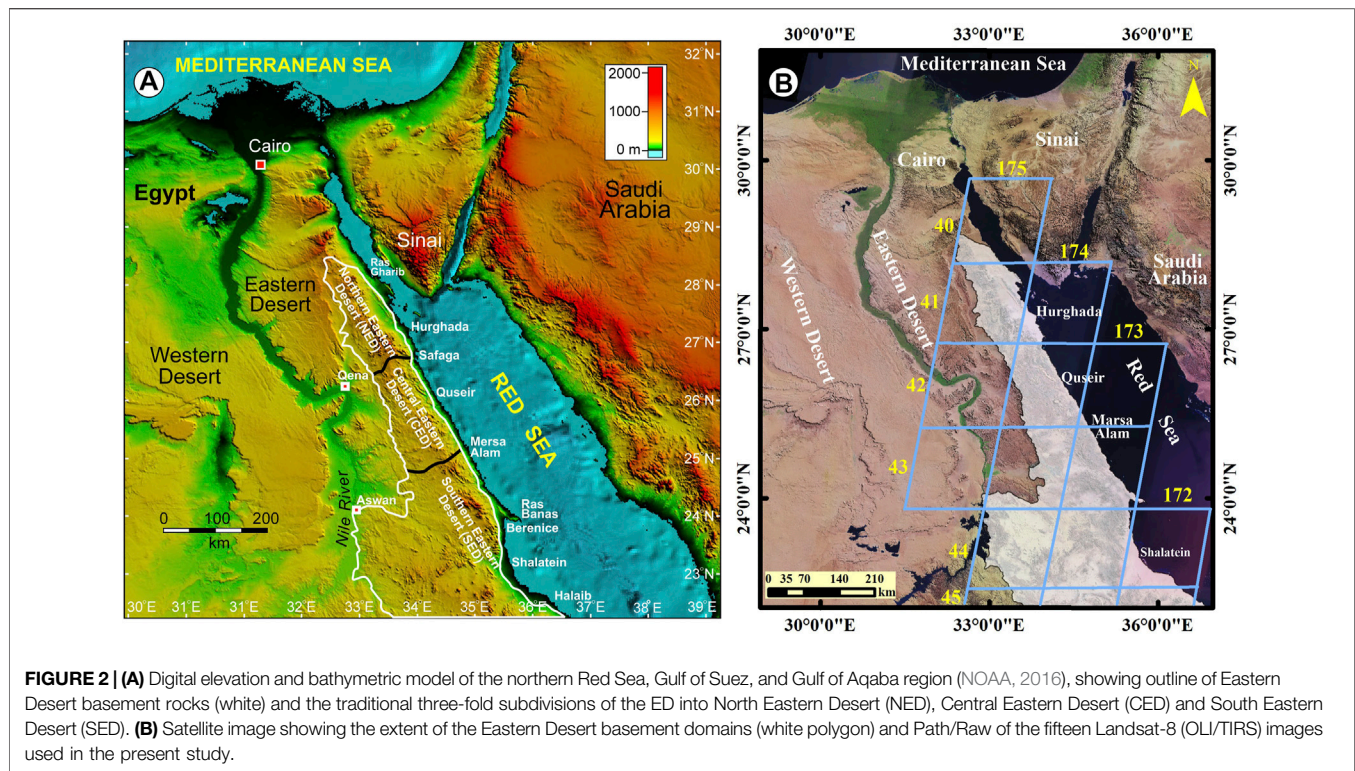


**FIGURE 1 |** Map of Northeast Africa and the Arabian Peninsula showing the distribution of juvenile Neoproterozoic crust and adjacent regions of Archean-Mesoproterozoic crust (after Fritz et al., 2013) and Cenozoic plate boundaries, Red Sea-Gulf of Aden spreading centers, and the East African Rift system (after Johnson, 2021). CED = Central Eastern Desert; NED = North Eastern Desert; SED = South Eastern Desert; SES = South Ethiopian shield; WES = West Ethiopian shield.

several lithotectonic units; 1) Gneisses and migmatites, 2) Ophiolites and island arc assemblages, 3) Syn-, late-to post-tectonic granitoids, and 4) Dokhan Volcanics and Hammamat Molasse Sediments. The Late Neoproterozoic belt of the ED is covered in the west by Late Paleozoic-Cretaceous sediments, collectively referred to as “Nubian Sandstone”.

## Gneisses and Migmatites

The gneisses and migmatites constitute the structurally deepest tectonic element of the Egyptian basement (infracrustal rocks or Tier 1, Bennet and Mosley, 1987; Greiling et al., 1994). These rocks are overthrust by ophiolitic nappes (supracrustal rocks or Tier 2, Bennet and Mosley, 1987; Greiling et al., 1994) along a



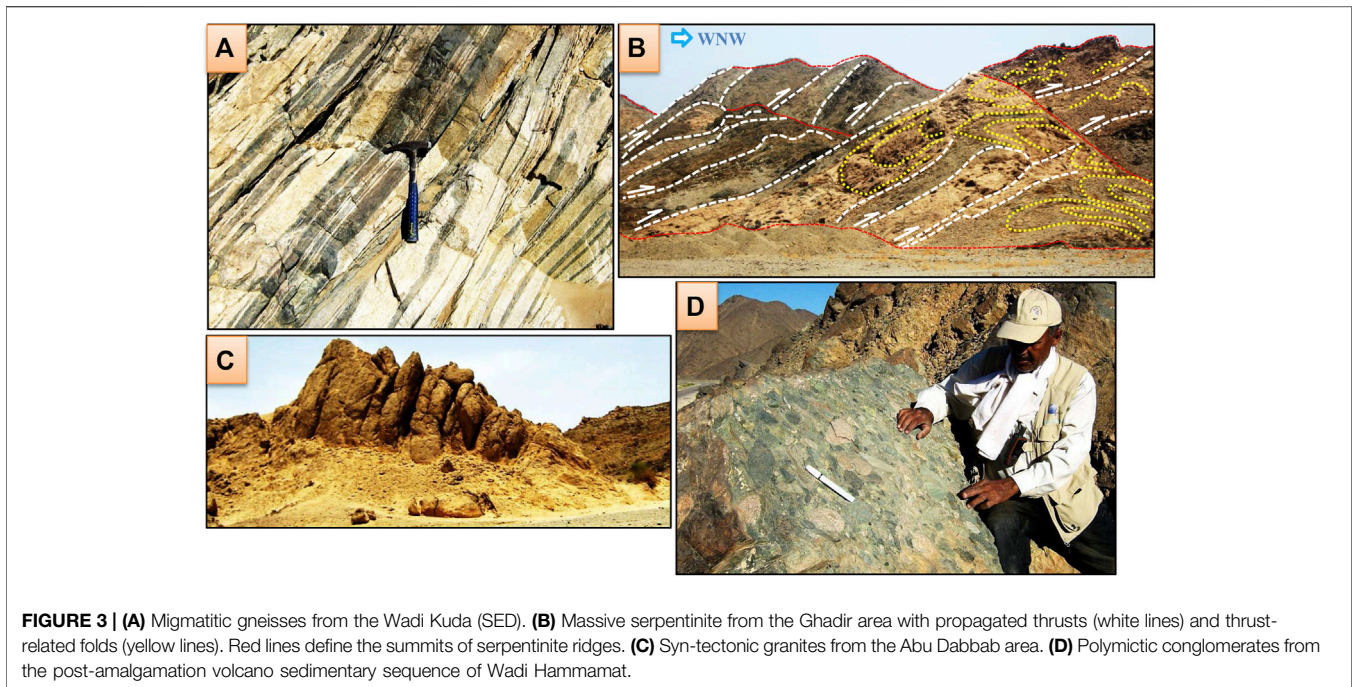
major detachment horizon. They are regionally metamorphosed up to the upper amphibolite facies and are mainly represented by schists, gneisses, and migmatites (**Figure 3A**). Earlier, these rocks were considered tectonic windows of “old” continental basement (El-Gaby et al., 1984) forming uplifted regions along the ENS and the entire ANS. The isotopic data of these gneisses rule out a pre-Neoproterozoic formation age. U/Pb zircon ages gave  $631 \pm 2$  Ma at Meatiq (Andersen et al., 2009);  $659 \pm 5$  at Migif-Hafafit (Lundmark et al., 2012);  $631 \pm 6$  Ma at El Shalul (Ali et al., 2012);  $725 \pm 9$  Ma at Beitan (Ali et al., 2015). These data further indicate that a depleted mantle source was the protolith for most of the crust of the ED (Liègeois and Stern, 2010; Augland et al., 2012). We interpreted these rock suites as representing deep-seated metamorphosed roots of arcs, probably delineating sites of individual island arcs. The gneisses and migmatites form conspicuous gneissic domes along the ED at Meatiq, Migif-Hafafit, El Sibai, and El Shalul, where they are structurally overlain by fold/thrust belts of supracrustal rocks. Such domes are bound at their NE and SW margins by NW-trending left-lateral strike-slip faults (e.g., Fritz et al., 1996) and occasionally by NW- and SE-dipping normal faults.

## Ophiolites and Island Arc Assemblage

The ED of Egypt contains many remnants of Neoproterozoic oceanic lithosphere in form of ophiolites, obducted during the Pan-African Orogeny (Stern, 1994; Stern et al., 2004). In most cases, the Egyptian ophiolites are variably dismembered forming tectonic melanges. However, local intact ophiolite sequences were documented (Wadi Ghadir ophiolites, El Sharkawi and El Bayoumi, 1979; Gabal Gerf ophiolites, Zimmer et al., 1995). The Egyptian ophiolites include

serpentinized ultramafics, metagabbros, and locally observed sheeted dykes (Gerf and Sol Hamed ophiolites; Gahlan, 2006), and mafic-metavolcanics that are sometimes pillowed and associated with ophiolitic metasediments. At their tectonic contacts, sole thrusts, and shear zones, the serpentinites (**Figure 3B**) and metavolcanic rocks are highly deformed and transformed into sheared-serpentinites and talc-schists, and metavolcanic-schists such as chlorite and actinolite schists, respectively. They form imbricate fan structures, thrust duplexes, and antiformal stacks of various scales and concentrate within CED and SED. The majority of ophiolites formed between 750 and 730 Ma in the Allaqi, Gerf, Ghadir, and Fawakhir areas (Zimmer et al., 1995; Ali et al., 2010). Different models have been proposed for the tectonic setting of the ED ophiolites. These include the formation of ophiolitic rocks in fore-arc basins (Gahlan et al., 2015), back-arc basins (Abd El-Rahman et al., 2009), or along mid-ocean ridges (El Gaby et al., 1984). Regardless of their specific setting, the ophiolites formed during the break-up of the Rodinia supercontinent represent the formation of individual basins within the wider Mozambique Ocean (Collins et al., 2021b).

In the Egyptian basement complex, the island arc-related rocks include intrusive as well as extrusive assemblages (Bentor, 1985; Abu El-Ela, 1997). The intrusive suites are represented by gabbro-diorites and tonalites, whereas the extrusive assemblage comprises volcanic rocks (mainly basalts and andesites) and volcano-sedimentary sequences. They have strong calc-alkaline affinity and are regionally deformed and metamorphosed up to the lower amphibolite facies. Like ophiolites, the island arc rocks are proposed to have been formed on the oceanic crust of the Mozambique Ocean (Johnson et al., 2011).



## Syn- and Late- to Post-Tectonic Granitoids (Egyptian Granites)

The granitic intrusions of the ENS are classically divided into “older” (gray) to “younger” (pink) granites (Akaad et al., 1979). Most probably, they originated from single or similar magma series that have evolved and fractionated from a mantle-derived magma (Moussa et al., 2008). These intrusions follow a geochemical trend producing earlier phases of calc-alkaline granites while the later phases were represented by alkaline to per-alkaline granites (Hussein et al., 1982; Ali et al., 2013). The older granites (**Figure 3C**) represent the first type, which comprises calc-alkaline granites that range in composition from granodiorite, and tonalite to quartz-diorite. In contrast, the younger granites define the second type with rock compositions including alkali feldspar granites, granites, and granite-adamellites (Ali et al., 2012). The third type of granites that have compositions ranging from alkali feldspar granites up to syenites are considered A-type granites (e.g., Moghazi, 2003). Older granites are syn- to late-tectonic and subduction related (Hassan and Hashad, 1990) representing a pre-collision arc-magmatic phase (Stern, 1994). The younger pink granites and A-type granites specify the late-orogenic to within-plate granitoids (post-tectonic), respectively (El-Bialy and Omar, 2015).

## Dokhan Volcanics and Hammamat Molasse Sediments

During the late orogenic history of the ED (~610–590 Ma), a stage of K-rich calc-alkaline volcanic activity evolved resulting in a variety of volcanic rocks (Dokhan Volcanics) ranging in composition from basic-intermediate to acidic volcanics and

related pyroclastics and tuffs (Abdel Rahman, 1996; Eliwa et al., 2006). These volcanic rocks are abundant in the NED and CED and rarely recorded in the SED. Dokhan Volcanics erupted before and coeval with the deposition of the Hammamat molasse sediments and are subjected to low-grade metamorphism (Ressetar and Monrad, 1983; Bretkreutz et al., 2010). The tectonic setting of the Dokhan Volcanics is debatable and various origins were proposed covering a wide range of tectonic regimes. These include compressional active continental margin (El-Gaby et al., 1989; Abdel Rahman, 1996) to intermediate (Eliwa et al., 2006) and extensional rift system (Stern et al., 1984).

Hammamat sediments are molasse-type sediments that evolved during the late stages of ENS evolution and the sedimentary environment as well as their composition allows retracing the sedimentary provenance as well as the exhumation history of sediment delivering units. In addition, the sediments act as a time marker for syn- and post-sedimentary tectonics (Fowler and Osman, 2013).

The succession of the Hammamat sediments consists mainly of greywackes and siltstones with polymictic-breccias and conglomerates (**Figure 3D**) at the lower part (El-Gaby et al., 1984; Willis et al., 1988). These sediments were locally subjected to thermal contact metamorphism due to emplacement of the late- to post-tectonic granites (El Gaby and Khudeir, 1988). The petrography and sedimentology of some of these basins, such as Wadi Hammamat, Wadi El Qash, Wadi Kareem, and Wadi Miyah basins have been investigated by Messner (1996) and Fritz and Messner (1999). Hammamat molasse basins are classified according to their location and the structural setting of each basin (Fritz and Messner, 1999; Abd El-Wahed, 2010). These include foreland basins, characterized by thrust-related

structures, such as Wadi Hammamat and Wadi Qash basins. Intermontane basins, markedly developed as pull-apart basins, like Wadi Queih and Wadi Igla basins, and intermontane basins, deformed merely by the strike-slip and extensional shearing, such as Wadi Kareem, Wadi Atawi and Wadi El Miyah basins. Basin formation through general N- to NW-oriented extension was proposed by Hassan and Hashad (1990), Abdeen and Greiling (2005), Shalaby et al. (2006), and Abd El-Wahed (2010). This is in accordance with strain data derived from pebbles (Fowler and Hamimi, 2021a, b) that gave NW-SE major principal strain axes in most of the basins.

## LANDSAT-BASED LITHOLOGICAL MAPPING

### Data and Methodology

The Landsat-8 data have been widely used for geological mapping and mineral exploration worldwide (Ali and Pour, 2014; Pour and Hashim, 2015; Mwaniki et al., 2015; Safari et al., 2017). In the present study, we obtained fifteen free cloud Landsat-8 level 1T (terrain corrected) images that covered the Neoproterozoic basement of the Eastern Desert of Egypt (**Figure 2B**) through the U.S. Geological Survey Earth Resources Observation and Science Center (EROS) (<http://earthexplorer.usgs.gov>). **Supplementary Table S1** lists the Landsat-8 characteristics and dataset attributes used in the present study. They were geometrically corrected and georeferenced to the Universal Transverse Mercator (UTM) projection (Zone 36 N), World Geodetic System (WGS) 84 datum, and ellipsoid. The fifteen images were processed using the ENVI 5.3 (ENVI® image processing and analysis software, from ITT Visual Information Solutions) and ArcGIS 10.5 (from ESRI® Environmental Systems Research Institute) packages. One raster image mosaic was made using the seamless mosaic module in ENVI 5.3. Masking of more than 115,350 km<sup>2</sup> of crystalline rocks belt was applied using shapefile in ArcGIS 10.5. Moreover, the atmospheric correction was considered one of the essential steps in the preprocessing phase (Lillesand et al., 2004; Chander et al., 2009; Tyagi and Bhosle, 2011; Abdelmalik, 2018). In the present study, we used the radiometric technique introduced in ENVI 5.3 to calibrate the Landsat-8 OLI images data for reflectance. In addition, the Digital Elevation Model (DEM) of the Shuttle Radar Topography Mission (SRTM) 1 arc-second with a 30 m horizontal spatial resolution was used to extract and visualize the structural elements through their topographical expression using the Geographic Information System (GIS) environment.

### Remotely Sensed Data Processing

Mineralogical and chemical composition, vegetation cover and weathering characteristics are important factors for lithological discrimination using remote sensing data (Xiong et al., 2011). The advances in these processing techniques have increased the accuracy of discriminated features. Therefore, image enhancements including color composites (true or false), band ratioing, principal component analysis (PCA), decorrelation

stretching, edge enhancements, and image fusion facilitated the differentiation and characterization of various elements in structural geology, mineralization, and rock types (Chen and Campagna, 2009; Gupta, 2013). In ED in Egypt, several studies have shown that appropriate image enhancements of remotely sensed data significantly improved the lithological discrimination and aided in field observations for lithological mapping. These studies pointed out that Landsat-8 with (OLI) sensor is considered one of the most effective data widely and successfully used for lithological mapping and exploration targets (Gabr et al., 2015; Hassan et al., 2015; Sadek et al., 2015; Asran et al., 2017; Aboelkhair et al., 2020; Hamimi et al., 2020). The Landsat-8 data, in combination with other remotely sensed data (e.g., ASTER and Sentinel) have been used to discriminate the exposed lithological units of ENS. These include the northern (Sadek and Hassan, 2009; Mohy et al., 2017), central (Sadek et al., 2015; Khalil et al., 2017; Mohammed et al., 2019), and southern (Zoheir and Emam, 2012; Hassan and Sadek, 2017; Emam et al., 2018; Mohy et al., 2019; Zoheir et al., 2019a, b) Eastern Desert of Egypt.

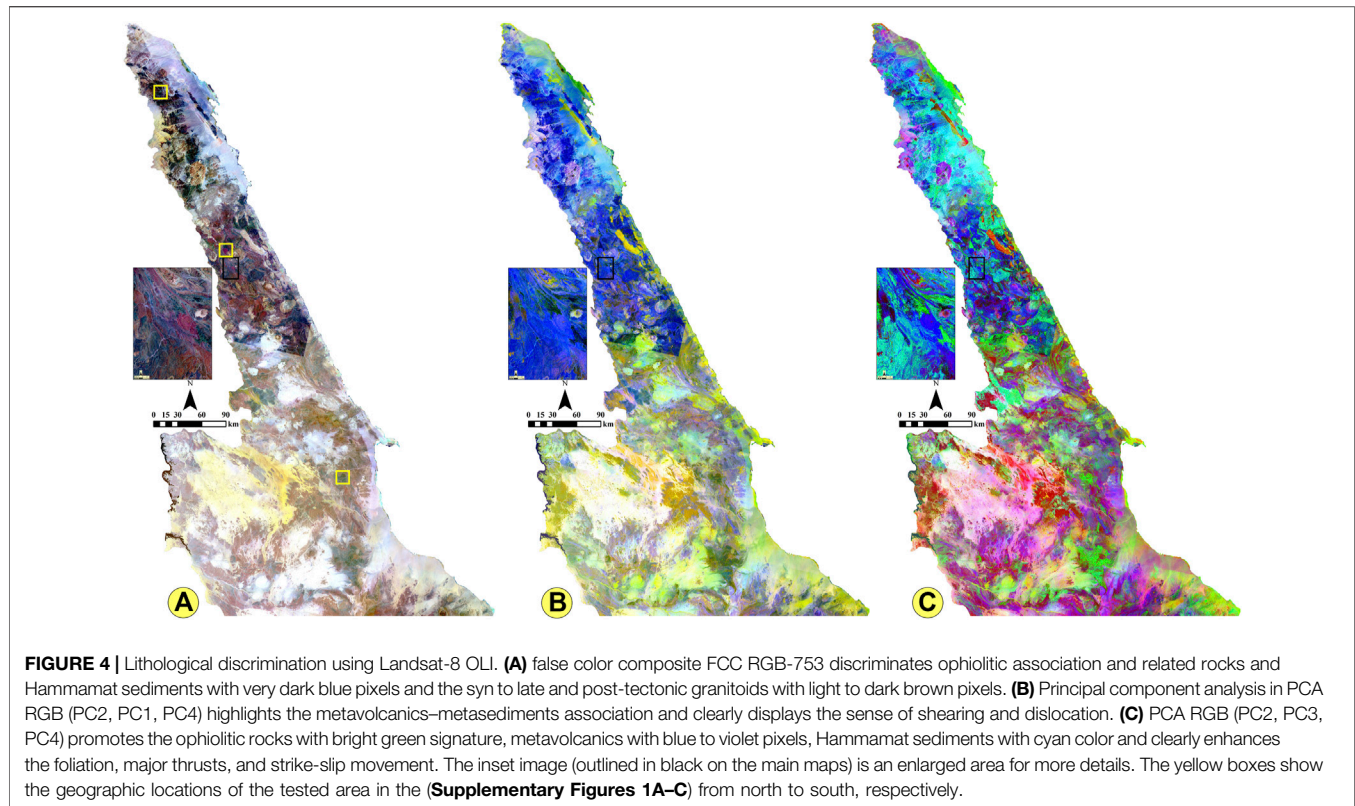
In the present study, several image processing techniques were applied to the Landsat-8 satellite data to generate a modified geological map with well-emphasized rock units and structural regions, which were verified by field observations of the entire ED. These techniques included color composites, band ratioing, mineral spectral indices, and Principal Component Analysis (PCA).

### False Color Composites (FCCs)

Color composites provide color variation images with different color tones that reflect the different spectral characteristics of the exposed rock units, as well as outline the structural features. Depending on the highest values of the Optimum Index Factor (OIF) (Chavez et al., 1982), the color composite of RGB-753 was selected in the present study (**Figure 4A**). This color composite provided a good illustration of the geological and structural features with a clear contrast of the different rock units and obviously traced the trajectories of the major structural elements in the Late Neoproterozoic belt in ED in Egypt. The serpentinites exhibited a mottled dark blue color in the thrust contact with volcanoclastic metasediments, which appeared as dull mixed dark green, dark gray to bluish-green and brown colors. The Hammamat molasse sediments were delineated as dark and light patches of brown areas. The granitic rocks were clearly outlined by brown color tones from light to dark. The image also displayed major fault contacts and shear zones that affected the rock units.

### Principal Component Analysis (PCA)

Principal component analysis (PCA) is one of the most effective and powerful image processing tools especially in geological mapping, such as for lithological, mineralogical, and structural applications. It is a multivariate statistical method for displaying the maximum contrast from several spectral bands with just three primary display colors (Vincent, 1997). This technique predicts whether a target is displayed as bright or dark pixels in different principal components based on the magnitude and sign of the



eigenvector loading (Jolliffe, 1986). In the present study, the eigenvector values of the Landsat-8 image were calculated and which displayed the highest amount of information in PC1 with 96.4 and in PC2 with 2.1. Zoheir et al. (2019a) demonstrated that the first three PCA images (PC1, PC2, and PC3), contained the highest topographical and spectral information and were suitable for lithological discrimination.

The RGB color combinations of Landsat-8 PCA were tested and adopted for mapping the lithological units and structural identification of the current study area. The RGB color composite of PC2, PC1, and PC4 exhibited the ophiolitic melange and associated rocks as grayish blue and the metavolcanics, metasediments, Dokhan Volcanics, and Hammamat sediments as blue tones from dark to light (**Figure 4B**). The felsic rocks exhibited light violet younger granites and lemon-yellow older granites. On the other hand, the ophiolitic rocks (serpentine and talc carbonates) were displayed as bright green patches in a distinct view in the RGB color composite of PC2, PC3, and PC4 (**Figure 4C**). The foliated metavolcanics and metasediments exhibited light purple colors whereas the Dokhan Volcanics and Hammamat sediments were displayed in cyan color. The granitoids appeared in light violet to yellowish violet colors.

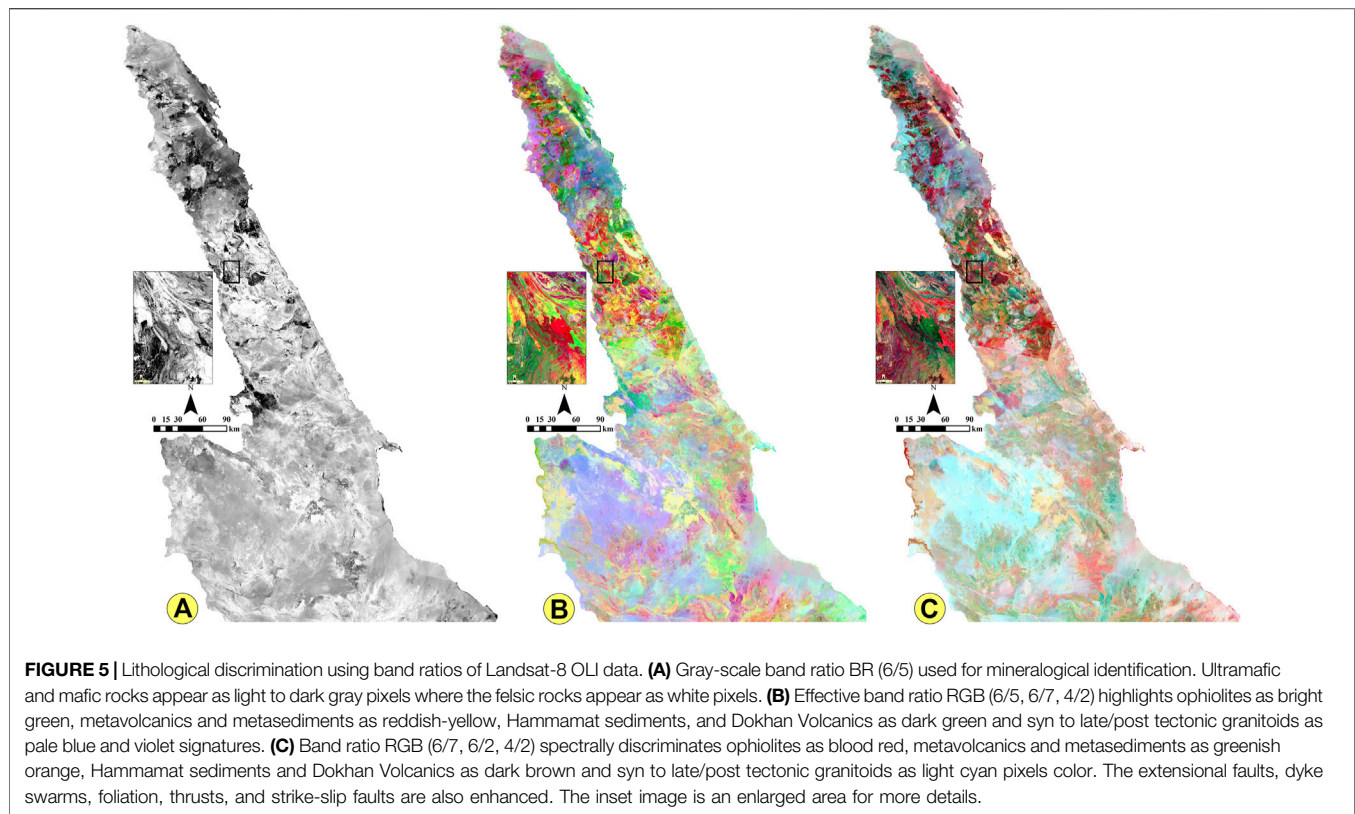
## Band Ratioing and Spectral Mineral Identification

The fact that each material displays a characteristic spectral reflectance curve that distinguishes it from other materials was

considered the base for the identification and discrimination of the different minerals and rocks from the remotely sensed data. Huntington (1996) stated that the hydrous mineral phases with OH groups (Mg-O-H, Al-O-H, Si-O-H) and CO<sub>3</sub> acid group possess diagnostic absorption features in the short-wave infrared region (SWIR) (2.0–2.50 μm). Therefore, the spectral signature was used to discriminate among the different minerals and rocks from the satellite images. In the same manner, numerous studies used band-ratio images to discriminate the different rock units based on their specific spectral characteristics. Therefore, band ratioing is considered one of the most important image processing methods for lithological mapping, and many researchers have applied the lithological and structural mapping in the ED in Egypt (e.g., Zoheir and Emam, 2012; Hassan and Ramadan, 2014; Hassan et al., 2015; Sadek et al., 2015; Abdelmalik and Abd-Allah, 2018; Abdelmalik, 2019; Zoheir et al., 2019a, b).

In the present study, Landsat-8 (6/5) was applied to display the ophiolitic and associated rocks as gray pixels, metavolcanics as light gray pixels, and Hammamat sediments as dark pixels and felsic rocks as bright colors (**Figure 5A**). Sultan et al. (1987) and Hassan et al. (2017) used a band ratio of (6/5) as an effective mafic index to enhance the meta-ultramafic and mafic rocks as light gray pixels.

To illustrate the detailed rock differentiation, the false color composites of some different band ratios were used to observe the variation in colors of the exposed rocks and facilitate their discriminations. Two main false color composites in RGB (6/5, 6/7, 4/2 and 6/7, 6/2, 4/2) (**Figures 5B, C**) were selected and processed to differentiate among the different rock units and demarcate the structural features in the study area. Image ratios



of (6/5, 6/7, 4/2) clearly discriminated the ophiolitic melange rocks (massive serpentinite and talc-carbonate schist) and gneisses with bright green and light green colors, respectively, the metagabbro and basic metavolcanics with dark green color and the Dokhan Volcanics with olive green colors (**Figure 5B**). The granitic rocks were shown in bloody red and light purple colors whereas the Hammamat sediments appeared in brownish dark-green colors. In addition, the major structural features (e.g., shear zones, thrusts, and strike-slip faults) were obviously demarcated by the variation of in the rock units' colors. The E-W and NW-SE strike-slip faults were clearly visible. On the other hand, image ratios (6/7, 6/2, and 4/2) are represented as the most powerful band ratio introduced in this study as a new band ratio for discriminating the rock units and structural features in more detail. The ophiolitic metaultramafics and related talc-carbonate rocks were obviously delineated with light and red dark purple image signatures (**Figure 5C**). The highly foliated gneisses and the metagabbros appeared as light and dark green colors whereas the metavolcanics and metasediments were displayed in orange green color. The Dokhan Volcanics and Hammamat sediments were shown in dark-brown tones. The vast array of granitic rocks was displayed in light-blue and creamy colors. Moreover, the foliation trajectories, folding, strike-slip faults, and thrusts were delineated by various colors. The aforementioned band ratios were more helpful and satisfactory in detailing lithological/structural mapping of the study area.

To outline the ophiolite assemblage and related rocks, the RGB color composite of PCA (PC2, PC3, and PC4) provided important

information about the ultramafic rocks and metavolcanics and metasediments association. The ophiolites appeared as deep blue intercalated with violet patches of metavolcanics and metasediments (**Figure 4C**). The intense foliation in the image delineated the ductile structures, especially in the southern part of the study area. The developed geologic map of ophiolites and related rocks (**Supplementary Figure S1A**) showed that these rocks were mostly distributed in the central and southern parts of the Eastern Desert. Thrust contacts, folding foliation, and strike-slip movement could be clearly observed from the differences in the color tones. The false color composite investigation of Landsat-8 (RGB-652) was performed to extract the felsic rocks in the study area as dark-brown, grayish-brown, and greenish-brown color tones. The granitic windows were well defined and separated from the surrounding rocks (**Supplementary Figure S1B**). Moreover, this composite successfully and clearly enhanced the regional foliation of the foliated rocks such as gneisses and migmatites and outlined the folded rocks as well as the major shear zones. This composite demonstrated the concentration of these rocks in the north Eastern Desert. The extensional features were enhanced by linear structures such as dyke swarms, jointing, and major strike-slip faults.

Finally, image processing of the Landsat-8 OLI data is an effective tool for generating a detailed lithological map, such as rock units and structural provinces, to approximately 115,350 km<sup>2</sup> of the Late Neoproterozoic belt in ED in Egypt. Because of the very large mapped area, some selected large-scale areas are shown in **Supplementary Figure S2A–C** to explore the power of remote sensing in enhancing the lithological contacts. The final modified

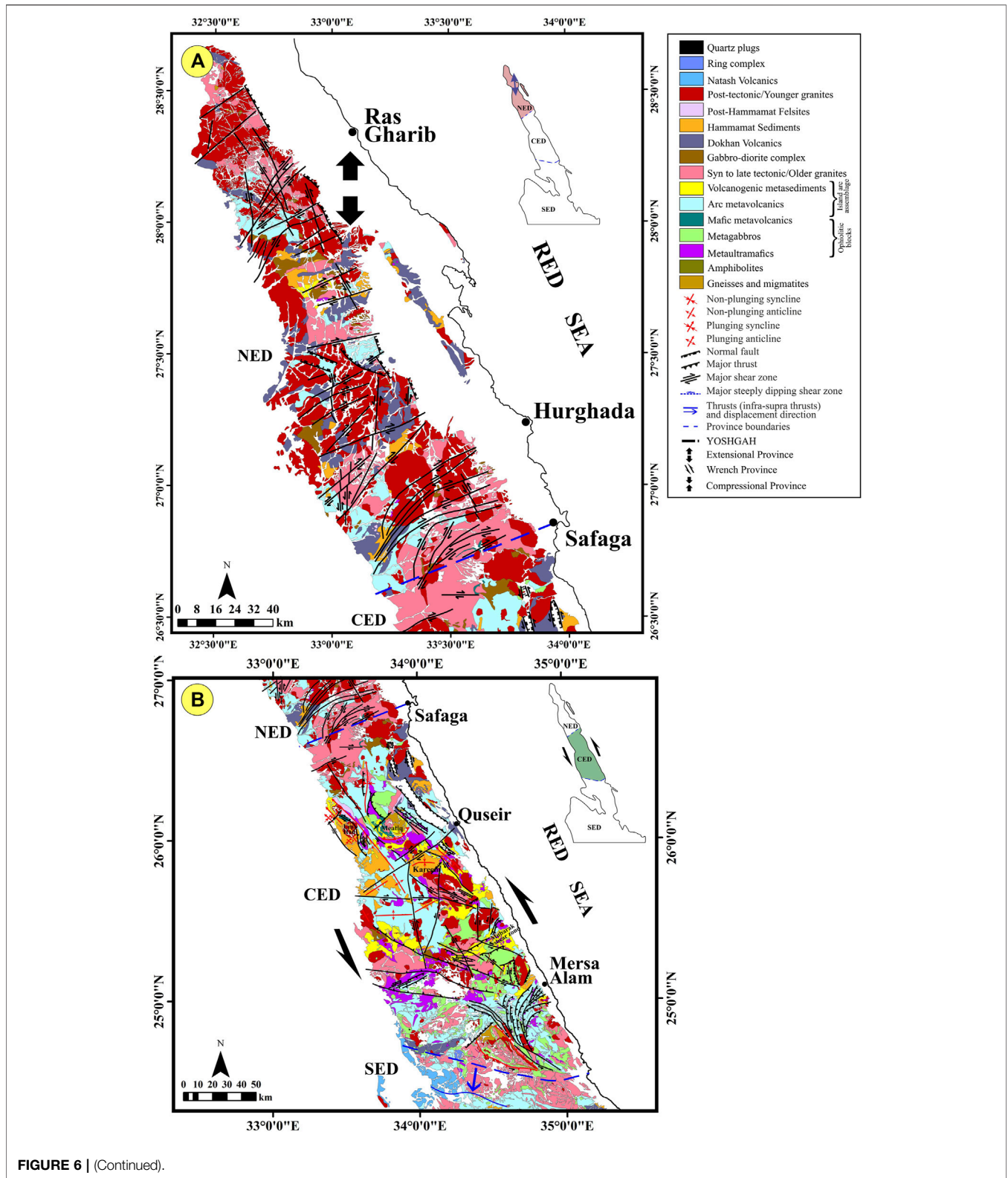
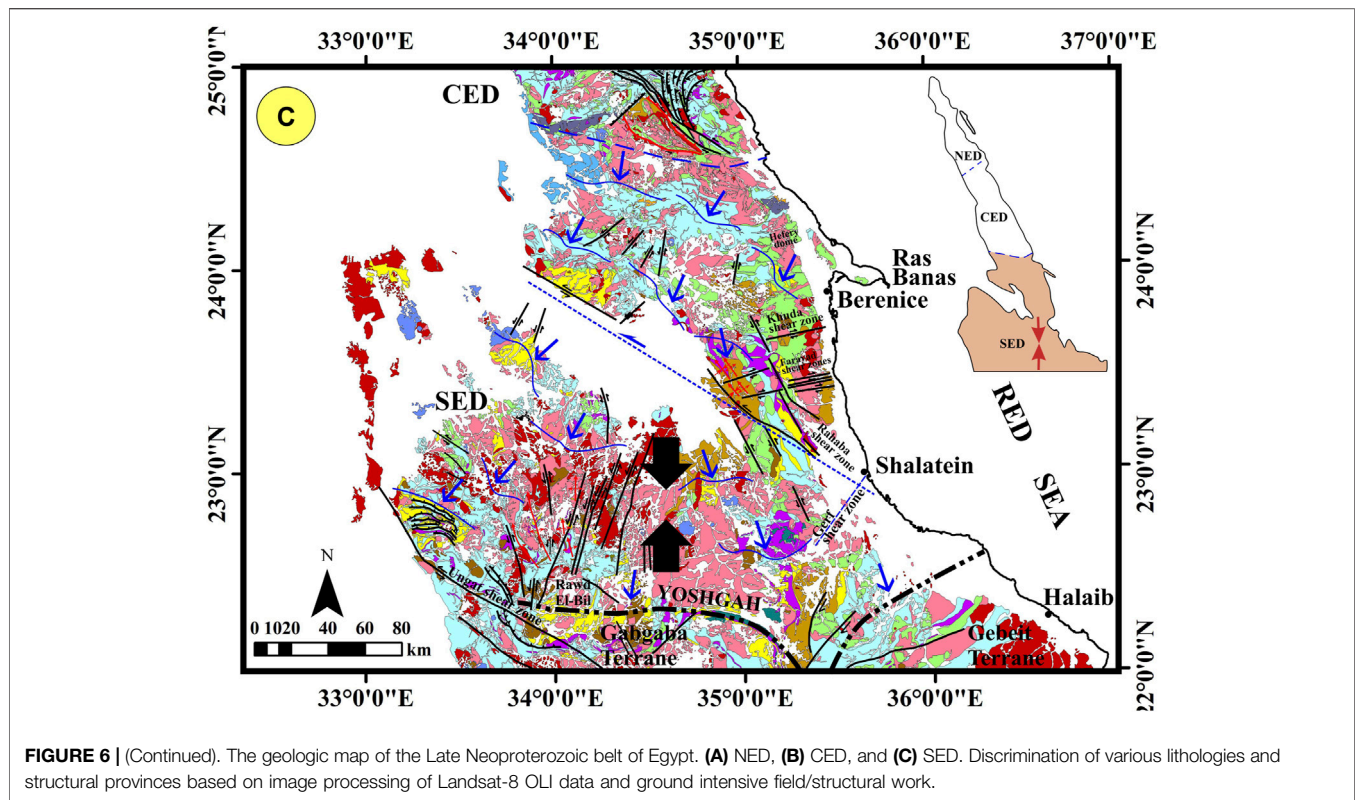


FIGURE 6 | (Continued).

geological maps are shown in Figures 6A–C. The output geological map was verified by using intensive fieldwork, observations in many localities in the study area, and correlation with previously published

maps. Random stratified samples were used to determine the overall accuracy assessment of the updated geologic map, which attained approximately 96.73% accuracy.



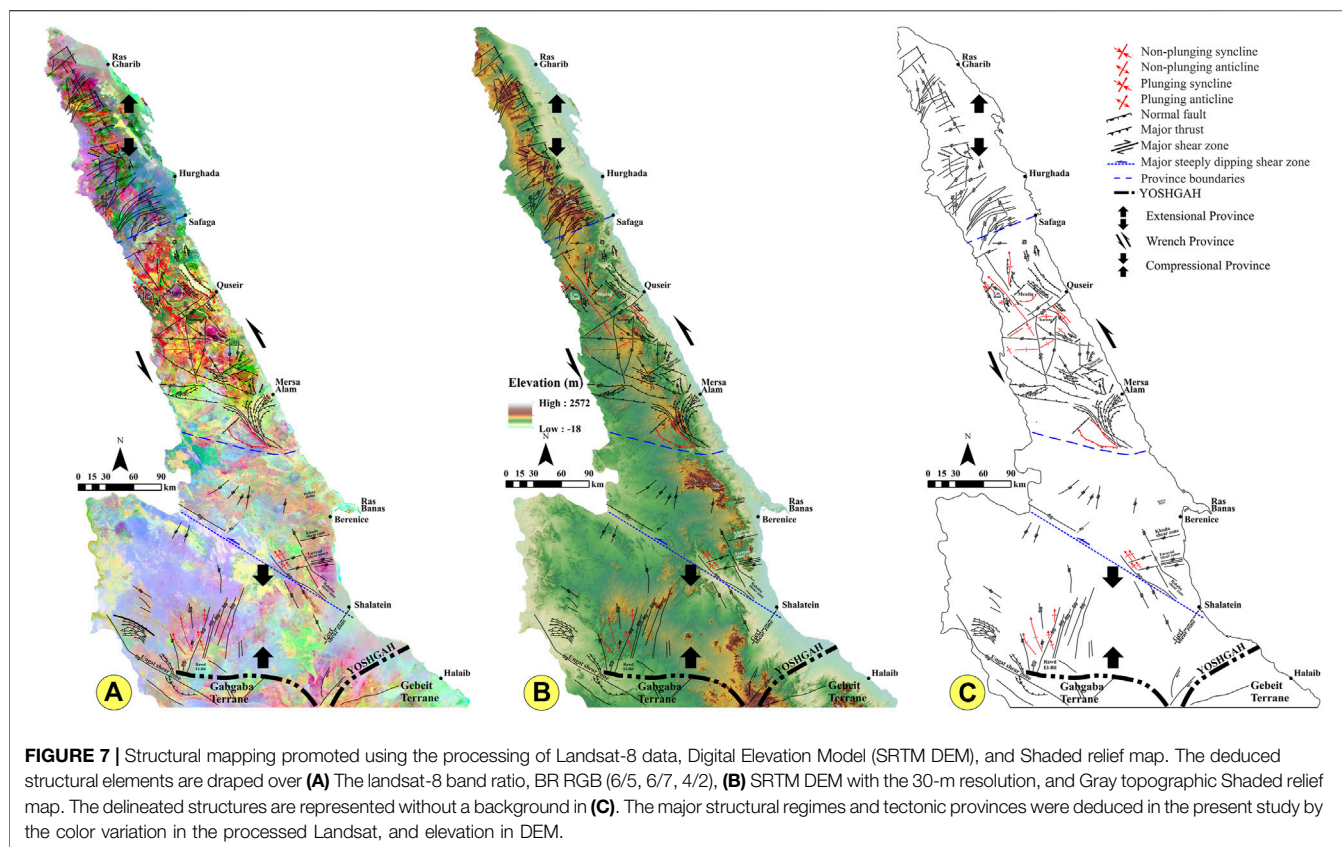
## Landsat-Based Structural Mapping

The remote sensing method offers the advantage of providing synoptic overviews of the structural features that extend over large areas. Identification of these structures is very efficient when the remote sensing data are integrated with computer-based GIS and verified by fieldwork. These data can be used to detect large geological structures such as shear and suture zones (e.g., Raharimahefa and Kusky, 2007, 2009). Faults can be demarcated using the topographic features with different orientations on DEM or by using the contrast and textural signatures in the remote sensing data. Homogeneous and kinematically consistent structural assemblages can then be used to define structural provinces, that most probably experienced similar tectonic histories. Zoheir et al. (2019a) recognized nine structural blocks in the Eastern Desert based on the differences in the structural trends. They inferred that the margins of these structural blocks were mostly major faults and shear zones and in some cases well-established or inferred suture zones.

In the present work, the interpretation of the structural provinces were based on the visual inspection of the tonal variation bright colors of the different rock types at band ratios of 6/5, 6/7, and 4/2 (Figure 7A). Moreover, the topographical expressions of the rock units, which appeared on the SRTM DEM (with 30 m spatial resolution) (Figure 7B) could enhance the tectonic boundaries and structural elements. The interpreted and detected structural elements are shown in Figure 7C. Depending on the analysis result of the extracted and previously published structural elements, the

architecture ED in Egypt could be divided into three major structural provinces (Figure 8). The major and minor brittle and/or ductile structural elements in the study area could be traced as shown in Figures 7A–C, 8. The analysis of these images, allowed us to distinguish the Neoproterozoic ductile and brittle structural assemblages. The traced structural elements overlapped the false color composites of band ratio (6/5, 6/7, 4/2) (Figure 7A, as an example). We emphasized that the well-developed foliations were dominant in the transpressional and compressional zones (ductile zone) of CED and SED. The zones accommodated major displacements and formed discontinuities that were considered transitional zones similar to those in CED. The considerable difference in the topography and foliation trajectories in provinces with ophiolite rocks relative to the arc metavolcanic rocks demonstrated distinctive deformation histories. NE-, E-W- and ENE-striking foliation and related close and overturned folds that extended for several kilometers were observed in the study area. The major NW, N-S, NE, ENE, E-W strike-slip faults adequately defined the differences in the color tones and rock units movements (Figure 7A).

The ability of remote sensing to extract the detailed structural features and kinematic indicators in the study area was investigated by selecting some examples for reference sites in NED, CED, and SED with small and large-scale areas. Four areas were selected to illustrate how remote sensing enhanced the structural elements (Figures 9A–H). Figures 9A, B shows ENE folded Hammamat molasse sediments, which exhibited —reddish brown pixels



intruded by granitic rocks (green pixels) and cross-cutting by the NW-trending strike-slip faults at G. El-Uref in NED. **Figures 9C, D** shows small-scale strike-slip faults that affected the sheared metavolcanics and metasediments at Wadi El-Miyah in CED. **Figures 9E, F** presents different folding styles that affected the Hammamat molasse sediments at the Hammamat Basin (Wadi El-Arak) and thrust ophiolitic rocks along the Atalla shear zone in CED. **Figures 9G, H** shows one of the most complex areas in the Wadi Allaqi in the South Eastern Desert. Compressional structures were conspicuous in this province and hydroxyl mineral zones mimicked the intensive foliation of the sheared rocks, which exhibited obvious ductile structures. The folded ophiolitic rocks were noticeably distributed adjacent to the variably deformed island arc metavolcanics and metasediments. These rocks were overthrust NW of the area. In addition, a series of NNW-oriented folds that are distributed and disrupted by the NE-striking faults was well observed and clearly traced.

## THE STRUCTURAL PROVINCES OF THE ENS

In the present study, the new tectonic map of the ENS encompasses a mosaic of three major structural provinces, namely, from south to north, compressional, transpressional/wrench, and extensional (**Figures 6, 8**). The discrimination of these provinces is based on the compatibility of the structural associations from the hand

specimen up to mountain scales that define the predominant tectonic regime. We concentrate on the major tectonic features and locate them onto a plate tectonic frame. For details, the readers are referred to the summary papers by Fritz et al. (1996), Abdeen and Greiling (2005), Abd El-Wahed (2007), Hamimi et al. (2019), Mohammad et al. (2019), Fowler and Hamimi (2020) and Hamimi and Abd El-Wahed (2020). The relative time constraints of the tectonic regimes are derived from the relationship between the rock formation and deformation. In the present study, we distinguish among the following 1) pre-Hammamat structural elements formed earlier than the sedimentation of the Hammamat molasse sediments, which are most likely related to accretion of the arcs and establishment of major decollement that separates infra-from supra-structures; 2) syn-to-late-Hammamat structural elements that evolved through the final collision and subsequent exhumation of metamorphosed arc roots; and 3) late-tectonic features that post-date Hammamat sedimentation and calc-alkaline magmatism (**Figures 6, 8**).

## Compressional Province

In the extreme southern portion of ED in Egypt, a prominent compressional province exists to the north of the Wadi Allaqi Shear Belt (part of the Greater YOSHGAH suture) that juxtaposed the Gabgaba-Gebeit Terranes against the Eastern Desert Terrane. The structures evolved as a consequence of a NNE–SSW contractional phase at c. 750–660 Ma. This province is characterized by WNW–ESE to W–E oriented thrust sequences,

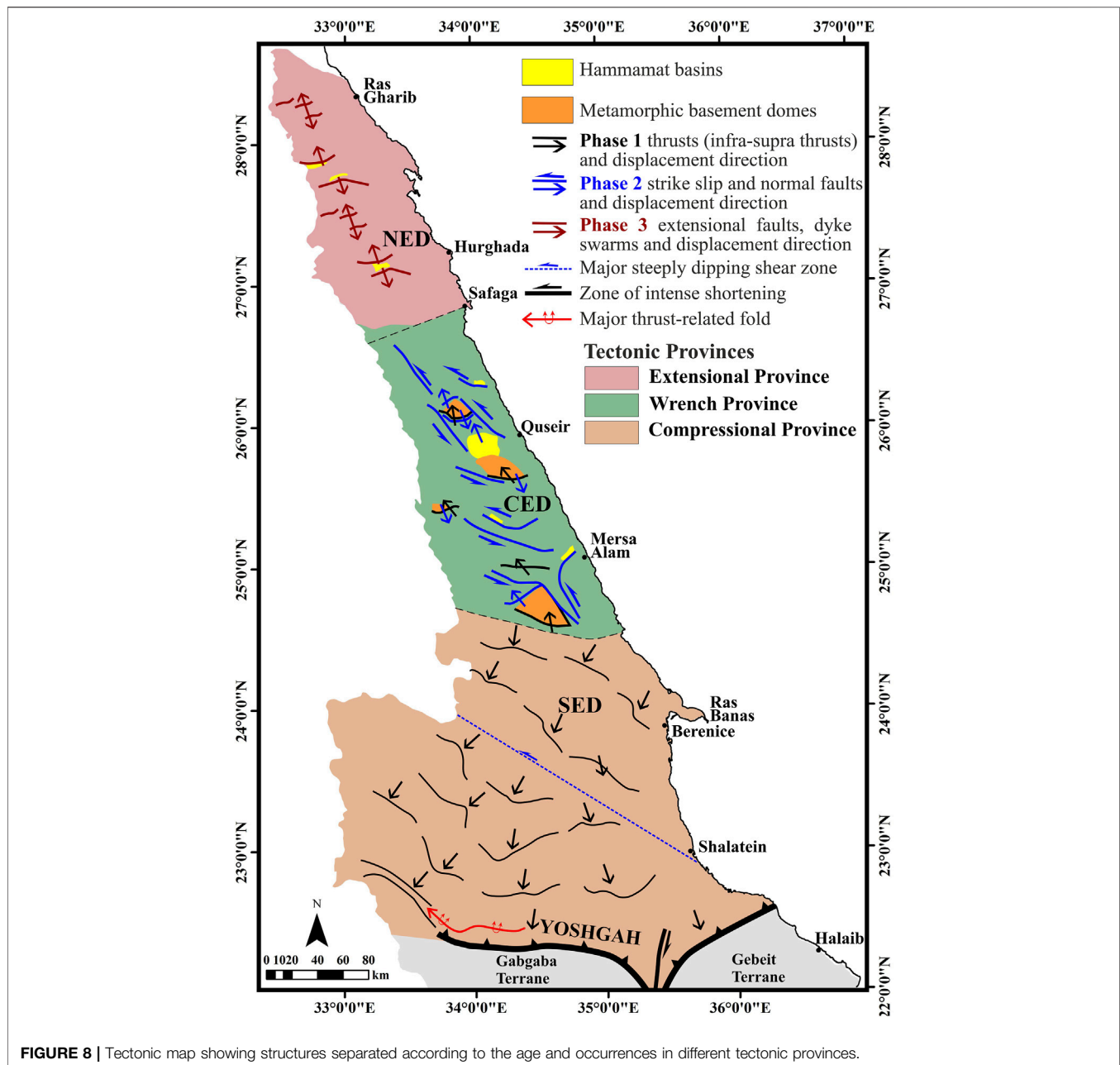
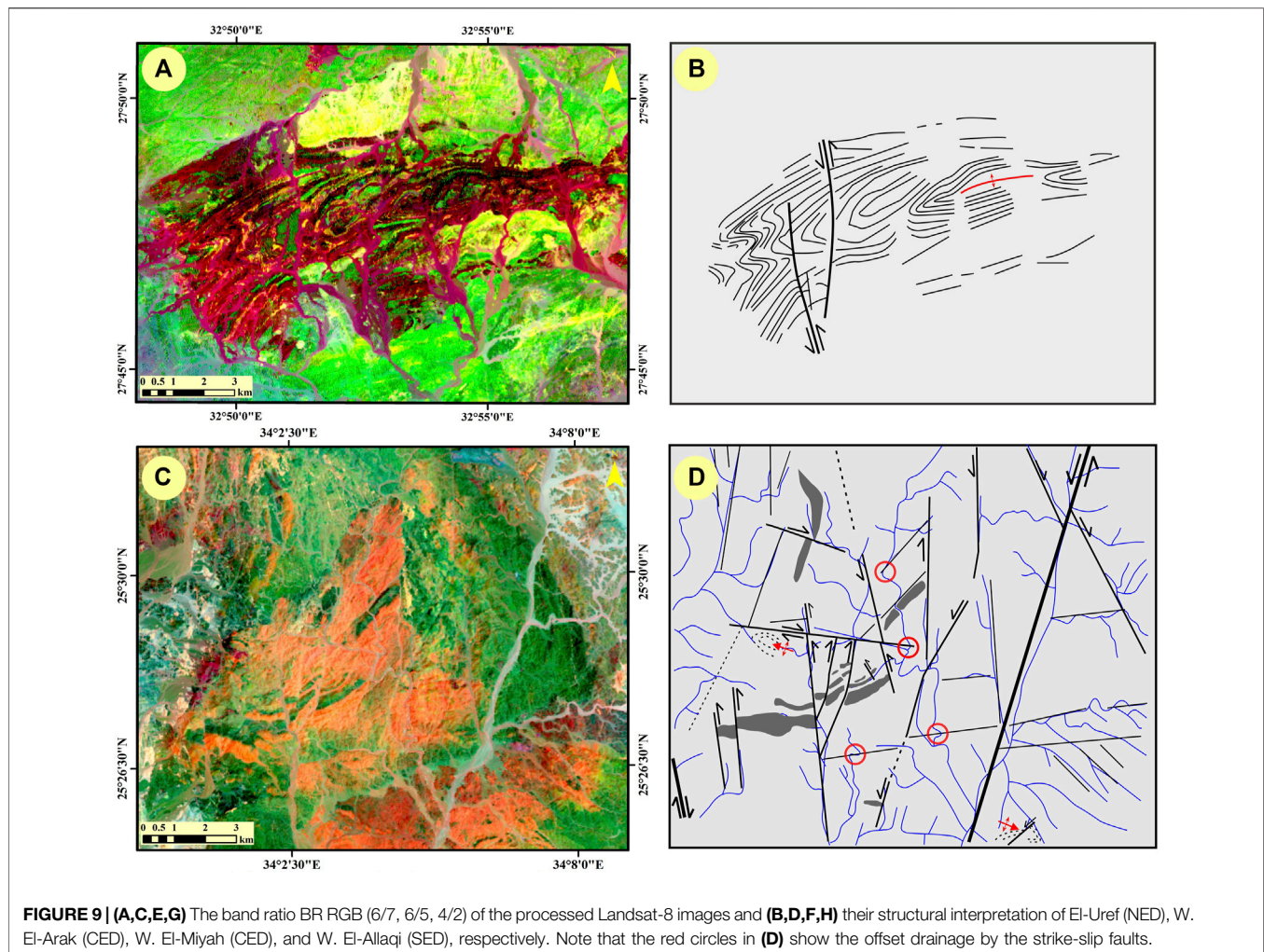


**FIGURE 8 |** Tectonic map showing structures separated according to the age and occurrences in different tectonic provinces.

which are best exemplified by those recorded to the west of Deneibet El-Koleib and near the Ungat shear zone (Figures 9G, H) and emplacement of the Gerf ophiolitic suite. The displacement of the thrusts towards SSW and S is responsible for the formation of well-developed thrust-propagation folds at Gabal Muqsim (Figure 10) and Um Shilman. The province extends northward to the Hafait basement dome but in the present study, an opposite sense of thrusting is shown (top N-NW) along NE-to-ENE-oriented thrusts. Further north, the top N-NW thrusting is preserved in the basement domes. The major decollement between the internal portions of these basement domes and the low-grade metamorphosed envelope of metavolcanics and ophiolite remnants are considered part of

this oldest compressional phase. In the current work, we believe that although the earliest structural elements dated back to c. 750 Ma, the SED compressional phase may have continued throughout the Late Neoproterozoic evolution in the ED. We also believe that although the conspicuous NNW-SSE trending Wadi Beitan major structure lies in this province, this structure was related to an earlier convergence between E- and W-Gondwanaland. The N-S shortening may be responsible for the refolding of this structure around the ENE-WSW (to E-W) direction. In this context, the remarkable transpressional shearing along the Wadi Kharit–Wadi Hodein belt (see Figures 7, 8) can be considered as the combination of the YOSHGAH shearing eco and the N-S contraction.



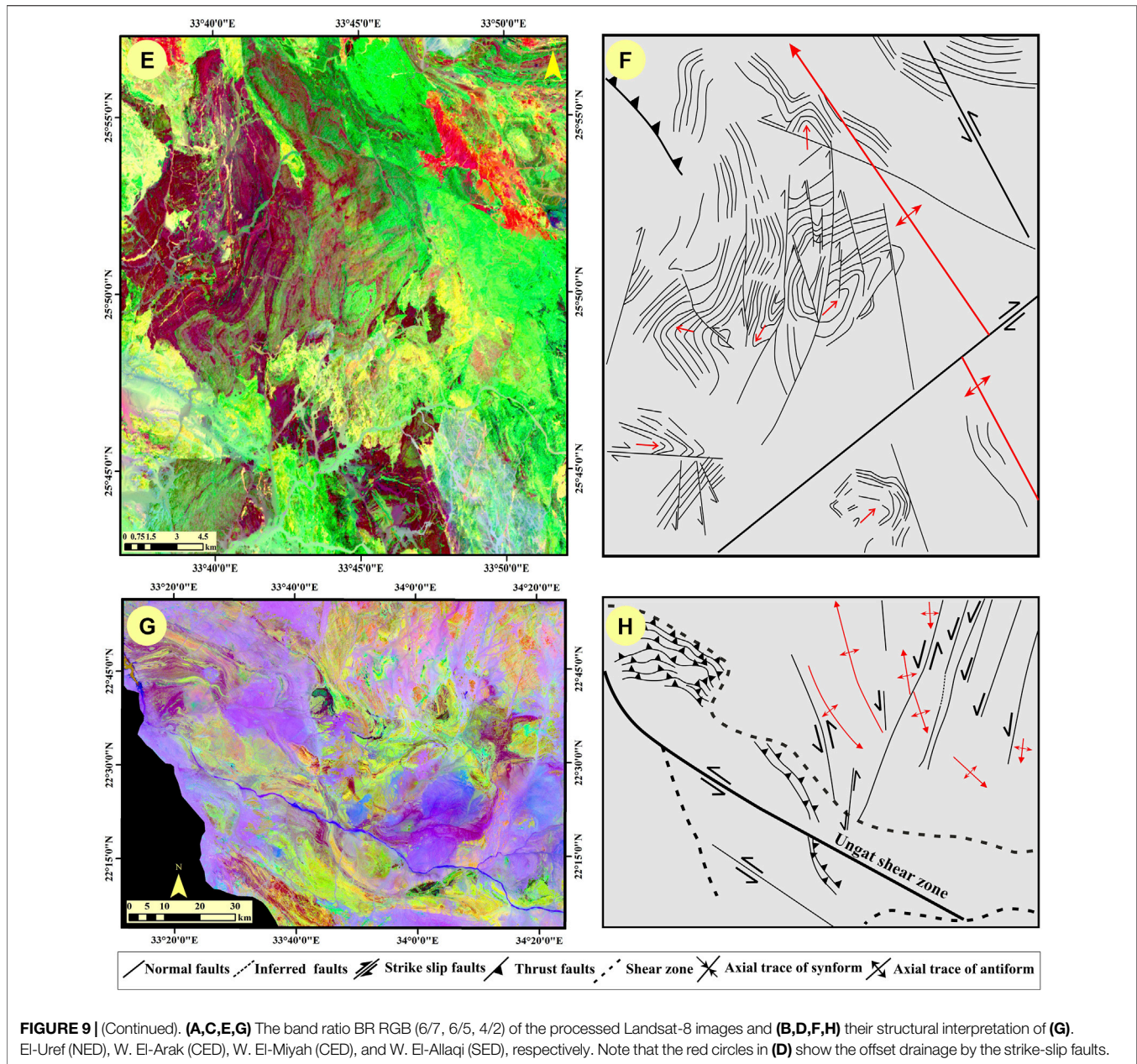
## Transpressional/Wrench Province

The transpressional province evolves between Marsa Alam in the south and Safaga in the north. This province includes large parts of the Najd Fault System and a transition zone that abuts the southern compressional domain. The compressional west-east-trending structures of the southern province are progressively overprinted by NW-SE-trending structural elements (**Figure 10**). The structures include NW-trending thrusts and folds in the external, western portions of the orogen such as in the Hammamat basin at the Quseir latitude. The main transcurrent belt is dominated by prominent NNE-SSW trending sinistral strike-slip shear zones. A number of cogenetic structural elements and rock suites evolve during this tectonic phase. The activity of the shear zones is associated with the coeval exhumation of metamorphic domes as evident from the  $^{40}\text{Ar}/^{39}\text{Ar}$  cooling ages of the domes (620–590 Ma) and the ages interpreted to represent a time of sinistral shearing (c. 590 Ma) (Fritz et al., 1996; 2002). The large shear belts adjacent to the Meatiq, Sibai, and Hafafit metamorphic domes, are most prominent, as better shown in the insets of **Figures 4, 5**, which show an enlargement of the Atalla Shear Belt (**Figures 11A–C**). Between the segments of

NNE-trending strike-slip faults, extensional bridges exhumed the domes through W-E trending normal faults. These extensional faults are formed at the margins of the Hafafit, Sibai, and Meatiq domes and indicate a significant component of the orogen parallel NNW-SSE extension. The extensional shearing is locally accompanied by emplacement of the syn-extensional granitoids (e.g., Abu Ziran granitoids to the south of Meatiq; Fritz et al., 2014) and is associated with the formation of the Hammamat molasse basins (e.g., Fritz and Messner, 1999; Abd El-Wahed, 2010; Fowler and Osman, 2013). Hence this structural association is clearly assigned “syn-to-late-Hammamat association”.

## Extensional Province

North of the Qena-Safaga Shear Belt lies a large extensional province that extends to the northern tip of ENS. This area is the site of voluminous post-orogenic magmatism (e.g., the voluminous granitoids of Gabal Shaeib El-Banat, Gabal Qattar, (**Figure 11D**), and Gabal Gharib, which is considered the result of mantle delamination and associated crustal thinning. Other evidence that supports the extensional regime includes the widespread E-W trending dyke swarms and the E- (to ENE-)



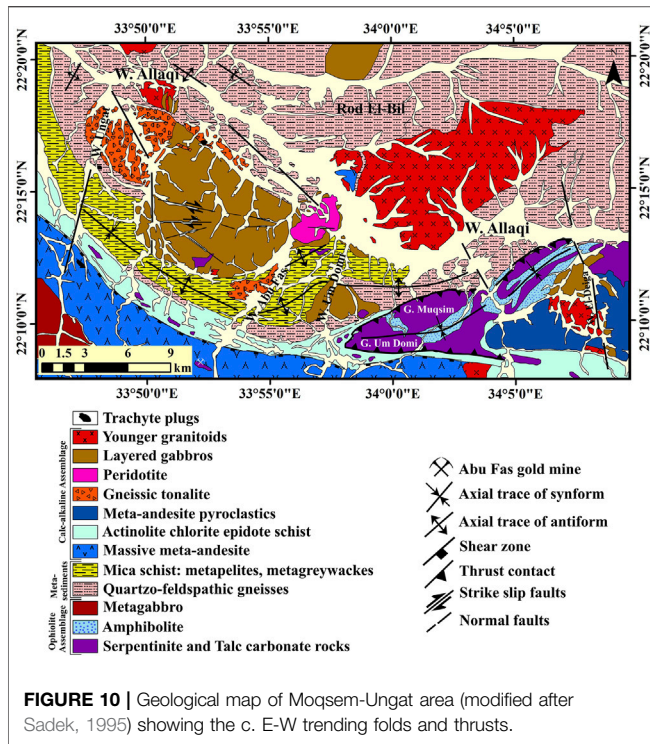
trending tensile fractures. Voluminous emplacement of the bimodal Dokhan Volcanics nearby the large granitoid masses is additional evidence of a late-stage extensional regime.

## DEFORMATION REGIMES AND FLOW FIELDS

### Deformation Regimes

Evidently, the deformation styles in the orogens are determined by the relative motion of the plates and changes in the plate motion, which are termed as “far-field boundary

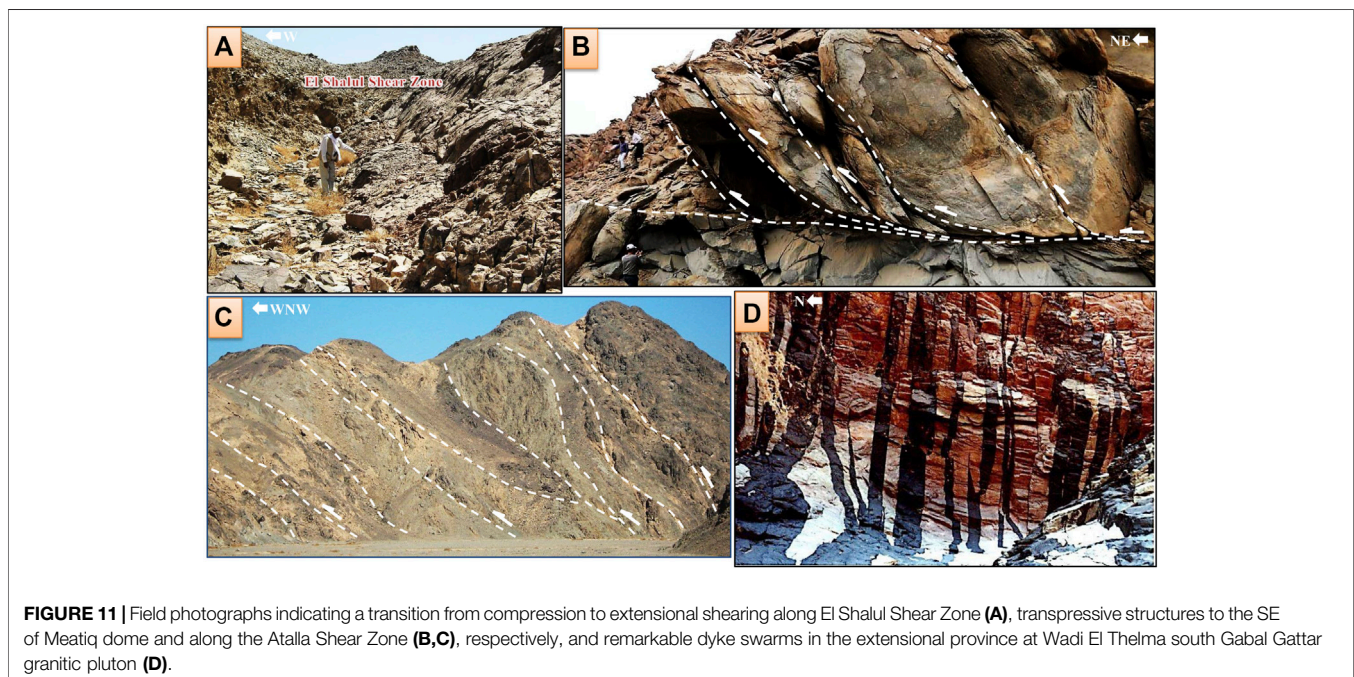
conditions”. It has been shown that oblique plate convergence has the potential to develop large strike-slip systems within the orogen, as exemplified by the Alpine Fault of New Zealand or the San Andreas Fault System of western North America (e.g., Norris et al., 1990; Titus et al., 2007; Mouslopoulou et al., 2009). Orthogonal convergence is, by contrast, characterized by an absence of large orogen-parallel faults, as seen in the central Himalayan or South American Andean systems (Xu et al., 2012; Armijo et al., 2015; Li et al., 2015; Horton et al., 2016; Hu et al., 2016). In the case of Late Neoproterozoic/Early Cambrian deformation events in the ED of Egypt, we suggest that three different far-field boundary conditions are



responsible to resolve the aforementioned structural assemblages. The earliest magmatic, metamorphic and tectonic history was released by the c. N-S convergence (recent coordinate system) of the Gabgaba—Gebeit, Jiddah—Asir terranes, and the Eastern Desert—Midyan terranes along the Allaqi-Heiani-Onib-Sol Hamid-Yanbo (YOSHGAH) suture between c. 800 and 620 Ma

(Figure 12). The second event, between c. 640 and 580 Ma, is believed to be related to the Nabatah Orogeny when the Afif-, Ad Dawadimi-Ar Rayn terranes of Saudi Arabia accreted to the earlier consolidated arc terranes (Afif and Tathlith terranes). E-W shortening in southern Saudi Arabia may have correlated with the N-S trending Hamisana Shear Belt of southern Egypt—northern Sudan. The northwestern Saudi Arabia and CED of Egypt simultaneously experience pronounced strike-slip deformation associated with displacement along wider NFS. This shear deformation offsets parts of the YOSHGAH suture through sinistral shear, namely the Yanbu suture segment. The third orogenic phase, which is younger than c. 580 Ma, is interpreted to be related to the evolution and retreat of the Cadomian Arc (Balleve et al., 2001; Bandres et al., 2002; Linnemann and Romer, 2002; Stern et al., 2016). The northern portions of ED in Egypt and Saudi Arabia have experienced extension and extensive post-orogenic magmatism.

As a working hypothesis, we suggest that the three different far-field boundary conditions controlled, with overlap, the structural assembly within three different domains in the ED of Egypt. Southern domains were influenced mainly by N-S convergence (Figure 13: far-field condition 1) and localized effect of W-E shortening (Figure 14: far-field condition 2) as seen in the activity within the Hamisana Shear Belt. The influence of far-field condition 1 diminishes northward but the influence of far-field condition 2 increases. The CED is considered a core area where Najd Fault-related structural elements developed. The far-field condition 3 dominates the northern segment of the ED as evident from extensive late orogenic magmatism and extensional fabrics (Figure 15). We relate the classical subdivision of the ED geology into NED, CED, and SED rather to external far-field boundary conditions than to activity of cryptic fault systems that remain proposed but unproven.



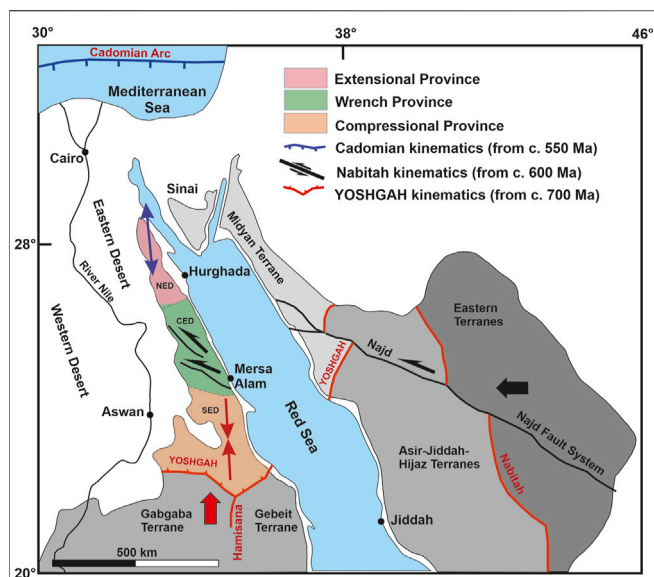


**FIGURE 12 |** Plate tectonic situation and structural provinces related to different plate kinematics. The earliest event, convergence, and collision between Gabgaba-Gebeit terranes and the Eastern Desert terrane along the YOSHGAH suture released north-south compression (thick red arrow) and related north and south directed thrusts (red double arrow) in the southern compressional province. West—east convergence (thick black arrow) associated with Nabitah Orogeny caused modification of suture and W-E compression in the Hamisana Belt. In the northern portion, this motion is partitioned into large sinistral strike-slip systems of the Najd Fault System leading to transcurrent motion within the CED wrench province (black half arrows). The retreat of the northern Cadomian arc enabled extension in the northern NED extensional province (blue double arrow).

## Flow Fields

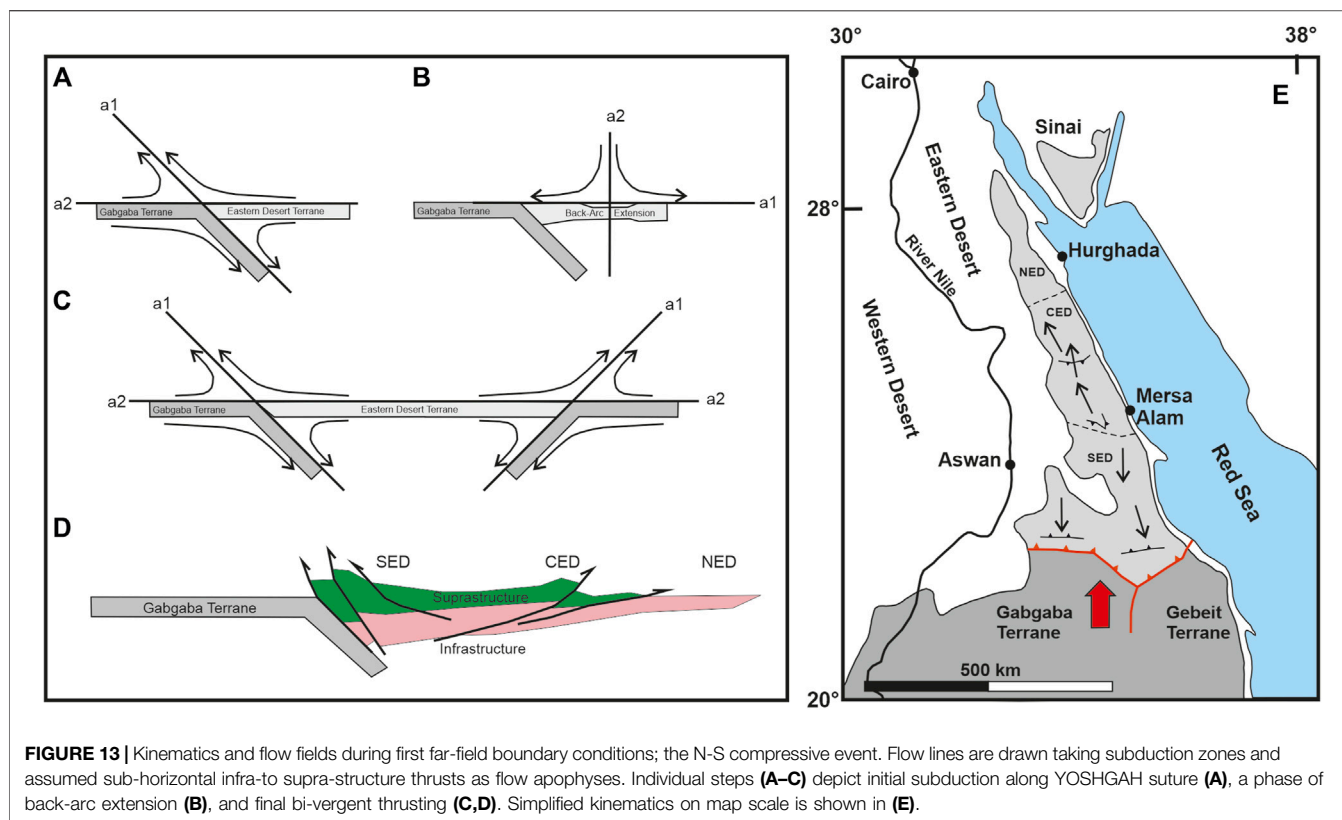
Far-field boundaries are simple, and associated structural assemblages are, however, complex. This is not only because of the superposition of successive deformation events but because deformation may partition into different components. The shape changes and particle displacement fields that characterize the flow of rock particles and thus the geometry of the structural elements are tensor quantities (second rank tensors). The displacement gradient tensor is related to the shapes of the initial to finite state and from the eigen-quantities of that tensor, the strain may be extracted. The velocity gradient tensor describes the way rock particles flow, the orientation of flow apophyses (eigen-vectors) provides information on the vorticity of the flow (Bobyarchik, 1986). This is expressed as a kinematic vorticity number, the nonlinear ratio between pure and simple shear components (for theory see Tikoff and Fossen, 1993). Conventionally velocity fields and displacement gradient tensors are derived from structural assemblages that are relevant to local situations. In Egypt, these kinds of data are rare. Here we use another approach and derive these quantities from the geometry and motion of plates. Plate motion vectors and plate boundaries, or high-strain deformation zones have shown to be parallel/contain the flow apophyses. Hence, from far-field boundary conditions, the flow fields may be derived when a homogeneous continuum is assumed (Tikoff and Teyssier, 1994). Considering these

assumptions, structural associations can be predicted and compared with observed structural elements. Below we display qualitatively the flow fields for the three different far-field boundary conditions suggested for the Neoproterozoic ED of Egypt.

These simple models are applicable for homogeneous continuum and isochoric deformation. A more realistic view has to implement concepts of displacement partitioning and strain compatibility (e.g., Tikoff and Teyssier, 1994; Teyssier and Tikoff, 1999; Jones et al., 2005). The concept of deformation partitioning states that the overall, over-regional geometry of a flow type maintains constant but may partition regionally. As soon as the vorticity in one domain is increased, for example through the activity of a simple shear zone, the vorticity in adjacent domains is reduced to keep the overall flow geometry constant. Hence, the presence or absence of a high-strain shear zone has a strong influence on the geometry of the structural assembly within and outside shear domains. The concept of strain compatibility states that geometries of bodies before and after deformation have to be compatible, common boundaries maintain and voids have to be avoided. This implies that deformation is not only determined by the overall induced stress field but also by the requirement to keep structural domains compatible. As an example, simple and pure shear (or general shear) deformations are not compatible with geometries. In progressive simple shear, the length of the shear zone boundary remains constant whereas this boundary is stretched in pure and general shear. To fulfill the requirements of strain compatibility either a fault has to be introduced between both domains or rock volume has to be removed or added.

## YOSHGAH Suturing—First Far-Field Conditions

Structural assemblages that are related to this event dominate the SED. Plate motion of the Gabgaba/Gebeit terranes relative to the Egyptian Eastern Desert terrane was largely orthogonal to the Allaqi-Heiani suture (Hamimi et al., 2019), western segments of the YOSHGAH suture system (Figures 12, 13). Hence minor lateral, suture-parallel motion is predicted and plane strain deformation is considered. The plane containing all relevant features including flow apophyses, instantaneous stretching axes, and strain axes is given by the plate motion vector and the normal trend of the suture zone. Flow apophyses were drawn parallel to the plate motion vector (eigenvector  $a_2$ : flow into the orogen) and parallel to the assumed dip of the subduction zone (eigenvector  $a_1$ : flow out of the orogen) (Figure 13A). The subduction zone dip was taken to be  $45^\circ$ , which corresponds to a general shear deformation with a kinematic vorticity number of  $c. Wk = 0.7$ . Schematically drawn flow lines show that expected structures include southward and upward emplacement of units within the Eastern Desert terrane with steepening of structures when approaching the subduction zone. This is in accordance with structural data from the SED which overwhelmingly displays top-to-south displacement (for a summary of data see Fowler and Hamimi, 2020). North-south trending lineaments (Figure 8) may represent tear faults accommodating differential shortening or



younger faults. As seen from **Figure 6C**, the SED is dominated by “Older Granites” and arc-related assemblages. Therefore, we argue that the structural setting described affected mainly the arc that developed in the back of the subduction zone.

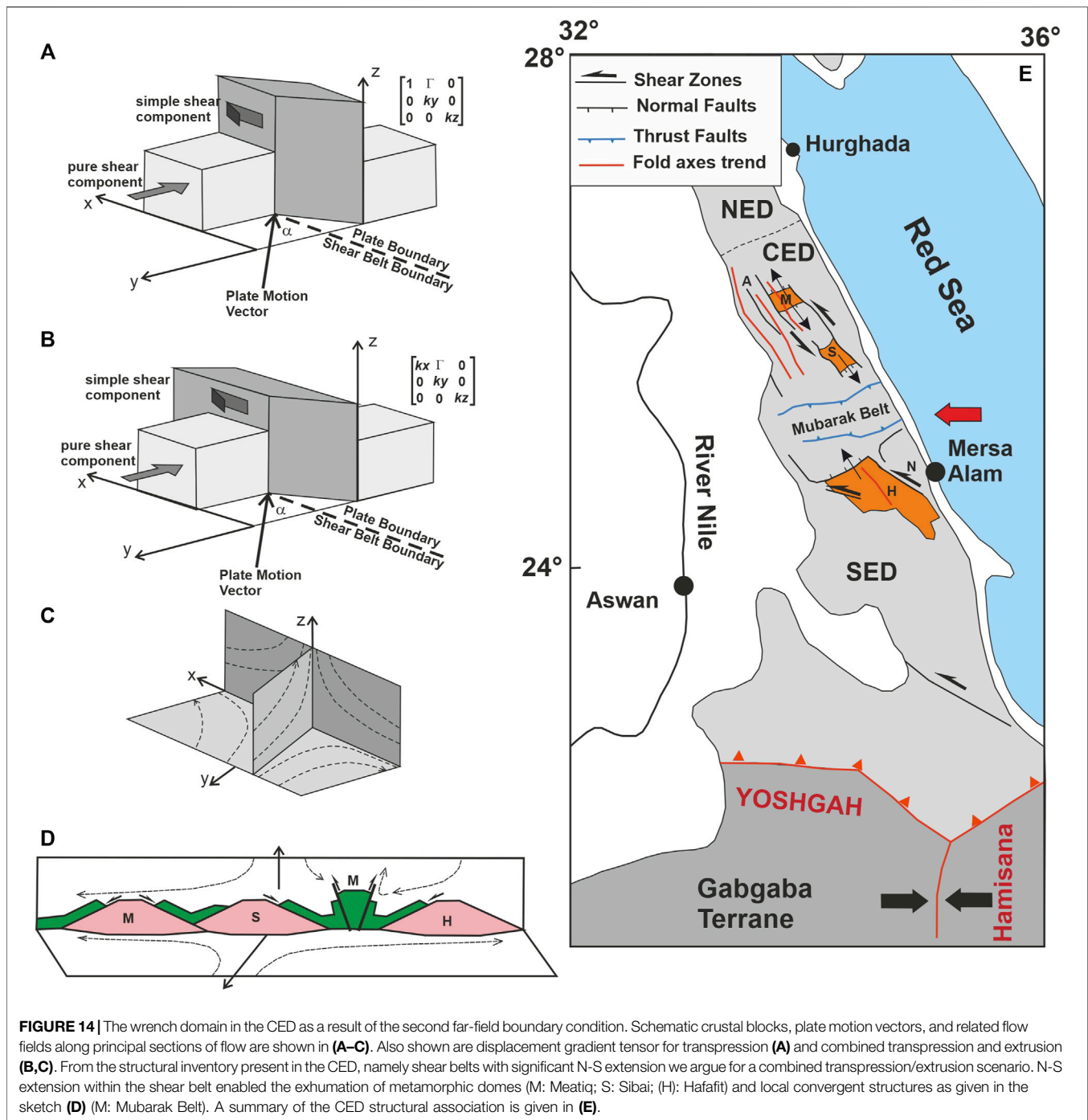
The CED differs in that it contains much more ophiolitic assemblages including mafic metavolcanics and ophiolitic melanges. Indeed, most authors favor the existence of back-arc and/or fore-arc basins separating older arc complexes (for discussion, see Fowler and Hamimi, 2020). This implies at least localized north-south extension to serve deposition of sediments between older arc assemblages and, when flow fields are considered, a shift in the flow apophyses. The flow apophyses parallel to the plate motion vector remain in the same orientation but become parallel to the extensional direction. The other one becomes subvertical ( $W_k = 0$ ), flow is now north-south and subhorizontal fabrics evolve (**Figure 13B**). Phases of north-south convergence and divergence may alternate before the final convergent phase and the closure of intra-arc basins. The sense of displacement in the CED is largely top-to-the north. It remains unclear whether this results from southward subduction in the CED or is the result of thrust and back thrust systems. We are convinced, however, that these structural elements, that is, south and north thrusting are related to the first far field condition and are responsible for the subdivision into tier 1, tier 2, or infra-supra-structure. Ophiolitic fragments and

melange were emplaced along flat thrusts over deeper roots of island arcs (**Figure 13D**).

## Nabitah Suturing—Second Far-Field Conditions

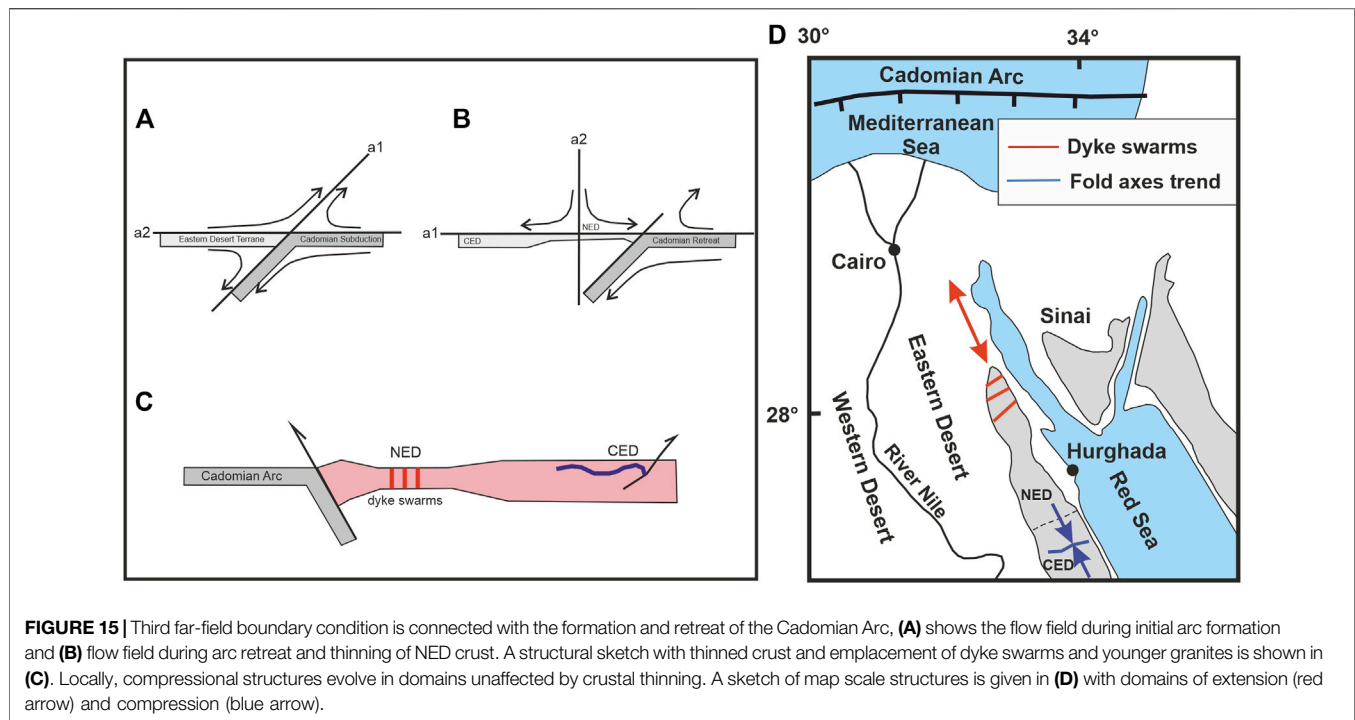
The structures related to this event evolved in Saudi Arabia as early as c. 680–640 Ma (Stoeser and Stacey, 1988); the major activity in Egypt was between c. 620 and 580 Ma, that is, after suturing of the Nabitah Suture (Collins et al., 2021a). Plate motion instigated activity of the crustal scale NFS, clearest seen in the CED (**Figure 12**). Fault activity falls into the time interval of cooling and exhumation of rocks now exposed in the Egyptian infrastructure domes (Fritz et al., 2002). Concomitantly, it occurred deposition and deformation of Hammamat molasse-type Basins (Abd El-Wahed, 2007; Fowler and Osman, 2013) and emplacement of shear related plutons (Fritz et al., 2014). Older structural elements, such as the infra-supra-structure tectonic boundary were overprinted and refolded.

From the geometry of involved plates and the plate motion vector, two domains are distinguished. Southern Egypt, to the north of the YOSHGAH suture, experienced orthogonal W-E convergence and shortening in the N-S-trending Hamisana Shear Belt (**Figure 12**). This belt is considered to represent a pure shear-dominated deformation zone (De Wall et al., 2001). Northern parts of Saudi Arabia and the CED, considered here in detail, experienced lateral displacement through oblique plate motion.



The flow field associated with Najd shearing is 3-dimensional. Full 3-dimensional calculation of flow fields is not only complex but also not very descriptive. Instead, it is convenient to look for special cases, such as transpression, lateral and vertical extrusion, or transtension, or to display flow fields in sections parallel to principal axes of flow (Tikoff and Fossen, 1999). Here we examine three possible strains and displacement scenarios and discuss the role of displacement partitioning. Flow and associated strain geometries during wrench tectonics could be transpressional

with subtypes of simple-shear- and pure-shear-dominated transpression, or combined transpression and lateral extrusion. Transpression in the strict sense as originally defined by Sanderson and Marchini (1984) can be ruled out. This is a pseudo-3D geometry that allows length changes in vertical ( $z$ ) and shear zone perpendicular directions ( $y$ ), but no change in length parallel to the shear zone boundaries ( $x$ ) as observed in the CED (Figure 14). The diagonal term in the displacement gradient tensor defining stretch parallel to  $x$  is 1 (Figure 14A).



Depending on the amount of accumulated strain and convergence angle of plates the long axes of the finite strain ellipsoid may be vertical or horizontal. At small angles of plate convergence up to  $\alpha = 10^\circ$  and finite strain ellipse ratios up to 100 (wrench dominated transpression) vertical foliation and horizontal lineation develops; at higher plate convergence angles  $\alpha > 20^\circ$  vertical foliation and vertical principal strain axes occur (Teyssier and Tikoff, 1999). Both scenarios are not compatible with the situation in the CED. The angle between the plate motion vector and the average trend of the NFS is  $30^\circ$ – $40^\circ$ . Thus vertical stretch is expected but stretching lineation along CED shear belts is, from field observation, subhorizontal. Hence, a component of lateral extrusion has to be added to fulfill the requirements of the observed vertical foliation and horizontal lineation. For a convergence angle of  $30^\circ$  and an assumed strain of  $R = 10$  (minimum) and  $R = 1,000$  (maximum) at least, 15–20% of lateral extrusion has to be added to reach these conditions (see graphs in Teyssier and Tikoff, 1999). This scenario is compatible with the structural assemblage observed in the CED as it enables vertical foliation, horizontal lineation, and components of horizontal and vertical flow (Figures 14B, C). In summary, the central part of the CED containing the NFS is a belt of pure shear dominated transpression combined with lateral extrusion.

Another important concept to explain structural associations within oblique convergent belts is that of displacement partitioning. Thereby, homogeneous flow patterns are decoupled, most probably along zones of strong rheological contrasts. Flow is no longer homogeneous, simple shear component concentrates in distinct shear zones, and the pure shear component in domains outside simple-shear domains. The amount of decoupling, that is, the percentage of slip partitioned on strike-slip faults can be quantified by comparison of structural

elements in- and outside-shear belts. In active orogens, measurements used to quantify partitioning are the flow apophyses derived from the plate motion vector and instantaneous stretching axes (stress) as obtained from active faults or borehole break-outs (Tikoff and Teyssier, 1994). This is not applicable in ancient orogens because all other elements except those parallel to flow apophyses change orientation during progressive deformation and strain accumulation.

A conspicuous feature of the CED is that almost all fabric elements are orthogonal to the Najd trend (for details see: Hamimi and Abd El-Wahed, 2020; Fowler and Hamimi, 2020). Fold axes trend parallel the shear zones and extensional faults occupy high angles to shear zones (Figure 14D). This could mean almost complete partitioning where the shear belts accommodated almost all of the simple shear components and coaxial fabrics evolved outside the shear domains. However, there are arguments pointing against such a scenario. The NFS itself is much more a broad belt with general shear deformation with much coaxial component than a distinct simple shear zone. Shear zone boundaries are stretched and when the extrusion component exceeds the shear component, horizontal shear may even reverse from sinistral to dextral. Structural elements at a high angle to the shear zones should rotate towards the extensional flow apophyses (a1). Observed normal faults, however, that could represent extensional bridges between branches of shear zones, such as the Nugrus–Hafafit shear extension system, have still high angles to the shear belt. Finally, the NFS in the CED is discontinuous and is transected by thrust belts at high angles to the shear zones. The most prominent of these belts is the W-E-trending Mubarak Belt with steep north- and south-dipping thrusts. In addition to these thrusts, prevalent dextral shear was taken as an argument to interpret the Mubarak Belt as

a conjugate shear system to the NFS (Shalaby et al., 2005; Hamimi and Abd El-Wahed, 2020). Here we offer another explanation for the Mubarak Belt and other high-angle shortening zones within the CED. Transpression and lateral extrusion within the CED were inhomogeneous in space and time; the component of NNW-SSE lateral extrusion was high but discontinuous. This is evident from the  $^{40}\text{Ar}/^{39}\text{Ar}$  hornblende cooling ages related to the shearing and exhumation of infrastructural domes (Fritz et al., 2002). Inner parts of the Sibai Complex exhumed and cooled below ca. 500°C at ca. 620 Ma. The northern Meatiq and the southern Hafafit Complexes cooled much later, at c. 580 Ma. This implies that the Sibai was a cold and rigid block representing a back-stop at the time when Meatiq and Hafafit complex exhumed through N-S extrusion. The extension was blocked by the back-stop and compressional fabric evolved next to the stiff block.

## The Cadomian Arc—Third Far-Field Conditions

From c. 590 Ma onwards northern Gondwana destabilized and crustal fragments drifted northwards assembling with today's Europe. The northward motion was accomplished through retreat of the Cadomian arc and extension in the back of the arc. Fragments of Cadomian crust (ca. 560 Ma) and eclogite (560–540 Ma) are now exposed in the northern Arabian Peninsula (Stern et al., 2016) and Anatolia (Canadian et al., 2016). In northern Saudi Arabia and northern Egypt, signs for slab retreat and possible mantle delamination are provided from extensive post-orogenic magmatism (younger granites) that concentrates in the NED (Figure 6A). The principal extension direction was approximately NW-SE based on the trend of 590–545 Ma dyke swarm trends in the NED (for a summary, see Abdel-Karim and Azzaz, 1995; Fowler and Hamimi, 2020). Shortly before the onset of retreat NED and CED may have experienced north-south shortening (Figure 15). This could explain the west-east-trending fold trends (Fowler and Hamimi, 2020) that post-date Hammamat sedimentation.

## THE PRESENT TECTONIC MAP VERSUS THE PREVIOUS MAPS AND CLASSIFICATIONS

Since the establishment of the Egyptian Geological Survey and Mining Authority (EGSMA), the geological mapping was rapidly growing over decades producing a vast literature of published and unpublished maps covering most of (if not all) the Egyptian territory. However, the previously constructed maps of the ENS suffered un-unified scale and map projection. These maps provide geological and structural data on limited and separate areas all over the shield. In addition, there wasn't an attempt to produce a tectonic map expressing such a name and subdivided the shield into tectonic provinces with an attached comprehensive review notes on the tectonic boundaries between the provinces. It also lacked to relate the structural elements that occurred within them to the major tectonic

events that deformed the ENS as a prominent part of the entire ANS.

The present study provides the first attempt to construct a tectonic map for the ENS in the ED utilizing the modern techniques of remote sensing and GIS, structural investigation, and re-evaluation of the previously published maps. The produced images and maps (Figures 4–7 and Supplementary Figures S1, S2) indicate that the remote sensing/GIS is a powerful tool in mapping lithological units of the Neoproterozoic basement complex of the ED. Also, remote sensing has successfully extracted detailed structural features and kinematic indicators which are reexamined in detail for some selected reference sites in NED, CED, and SED (Figures 9A–H). The final image processing of Landsat-8 OLI and DEM data is a comprehensive geological map (Figures 6A–C) with detailed lithology and structural features and a structural map (Figure 8). This figure shows the structural architecture of the ED is divided into three major provinces with the tectonic boundaries, major structures, and dominated tectonic regimes.

On the new tectonic map, the Neoproterozoic belt of the ED is subdivided into three structural provinces; Northern, Central, and South Eastern Deserts. These provinces are interpreted in terms of the different far-field boundary conditions between the tectonic plates/terraces. These boundary conditions controlled the assembly of structures within the ED structural provinces with an overlap at their transitions. The southern domain of the ED (SED) was influenced by the N-S convergence between Gabgaba—Gebeit, Jiddah—Asir terranes, and the Eastern Desert—Midyan terranes along the Yanbo-Onib-Sol-Hamid-Gerf-Allaqi-Heiani (YOSHGAH) suture (800–620 Ma). The central domain (CED) is the core of the belt where the Najd Fault-related structural elements developed between c. 640 and 580 Ma. It ascribed to the Nabitah Orogeny when the Ad Dawadimi-Ar Rayn terranes (eastern Arabian Shield) accreted to the earlier arc-related Afif and Tathlith terranes. In the northern segment of the ED (NED), the extensive late orogenic magmatism and extensional fabrics were dominated and controlled by the evolution and retreat of the Cadomian Arc (younger than 580 Ma).

The classical subdivision of the ED into NED, CED, and SED (Stern and Hedge, 1985; El-Gaby et al., 1988) was focusing mainly on the differences in lithology along with the unclear structural boundaries between the three domains. These boundaries follow the route of the main asphaltic roads that were suspected as major shear zones (the Qena-Safaga and Idfu-Mersa Alam shear zones) although they apparently do not cut through the exposed lithological units at their vicinity. The main advantage of the new tectonic map in the present study upon such previous classification and the previously published maps of EGSMA and CONOCO is the integration of the deformation regimes and flow fields (Figure 12–15) in the subdivision of the Egyptian Shield into provinces.

In general, the proposed tectonic map will open the door to a serious challenge to modify and even discard some old models and classifications on the ENS and help the better understanding of the lithologic units and affected structures. It will also allow to follow effective methods and approaches for re-evaluating the

local structures and tectonic setting in terms of the given far-field boundary conditions, tectonic regimes, and intraplate flow fields.

## CONCLUDING REMARKS

The results obtained from the present study can be summarized as follows:

- A new tectonic map has been developed based on intensive field/structural work, which is integrated with processing and analysis of the optical sensors using remote sensing techniques, and careful re-examination of the previously published geological maps and literature.
- ENS is subdivided into three structural provinces; compressional-, transpressional- and extensional-provinces. The proposed provinces are ascribed to three different far-field boundary conditions.
- The first kinematic event (between c. 800 and 620 Ma) was released by the c. N-S convergence of Gabgaba—Gebeit, Jiddah—Asir terranes and Eastern Desert—Midyan terranes along the YOSHGAIH suture. Several lines of evidence illustrate such convergence, the prevailing compressional regime in the vicinity of the Allaqi-Heini belt and the extreme SED in Egypt.
- The second kinematic event (between c. 640 and 580 Ma) was released by the Nabitah Orogeny when the Ad Dawadimi—Ar Rayan terranes of the Eastern Arabian Shield accreted to the earlier consolidated arc terranes (Afif and Tathlith terranes).
- W-E shortening in southern Saudi Arabia may be correlated to the N-S trending of the Hamisana Shear Belt.
- Northwestern Saudi Arabia and the CED of Egypt suffer from pronounced strike-slip deformation associated with the displacement along the wider NFS.
- The third kinematic event (younger than c. 580 Ma) was released by the evolution and retreat of the Cadomian Arc. The main effects of this event are remarkable extension, mantle delamination-related widespread postorogenic magmatism, associated crustal thinning, and E-W trending dyke swarms. It is well represented in the northern sectors of the ENS and the Midyan terrane in the northern Arabian Shield.
- The classical tripartite subdivision of the ED geology into NED, CED, and SED is related to the external far-field boundary conditions instead of the activity of cryptic fault systems that were proposed but have not been proven.

## REFERENCES

- Abd El-Rahman, Y., Polat, A., Dilek, Y., Fryer, B., El-Sharkawy, M., and Sakran, S. (2009). Geochemistry and Tectonic Evolution of the Neoproterozoic Wadi Ghadir Ophiolite, Eastern Desert, Egypt. *Lithos* 113, 158–178. doi:10.1016/j.lithos.2008.12.014
- Abd El-Wahed, M. A. (2007). Late Pan-African Tectonic Evolution and Strain Determination in the Late Neoproterozoic Molasse Sediments, Eastern Desert, Egypt: Evidence for Post-hammamat Compression and Transpression. *Egypt J. Geol.* 51, 1–39.

## DATA AVAILABILITY STATEMENT

The original contributions presented in the study are included in the article/**Supplementary Material**; further inquiries can be directed to the corresponding author.

## AUTHOR CONTRIBUTIONS

ZH, WH, HF, HB, and SK contributed to conceptualization, fieldwork, writing the draft manuscript, data processing, and software manipulation. All authors have read and agreed to the published version of the manuscript.

## ACKNOWLEDGMENTS

The authors would like to thank ND, IE, and MA for valuable comments that were significantly improved the original version of the manuscript.

## SUPPLEMENTARY MATERIAL

The Supplementary Material for this article can be found online at: <https://www.frontiersin.org/articles/10.3389/feart.2022.921521/full#supplementary-material>

**Supplementary Table S1** | Landsat 8 OLI/TIRS characteristics and the scenes used in the present study (after US Geological Survey, 2016).

**Supplementary Figure S1** | (A) Ophiolitic rocks and metavolcanic-metasediments association mapping promoted by the principal component analysis image PCA RGB (PC2, PC4, PC5) of landsat-8 OLI which represents the geographic distribution of serpentinites, ophiolitic metagabbros, mafic and arc metavolcanics and volcanoclastic metasediments in the Egyptian Nubian shield. (B) Gneisses and granitoid rocks mapped using the processed false color composite (RGB-753) of Landsat-8 OLI which showed the distribution of the gneisses rock in the South Eastern Desert, syn to late granitoids are mostly presented in the Central and south Eastern desert where the post-tectonic granitoids are dominated in the extensional province at the North Eastern Desert.

**Supplementary Figure S2** | Detailed lithological mapping of some selected areas in the ENS in the Eastern Desert using different image processing techniques such as false color composites (FCC), band ratios (BR), principal component analysis (PCA) to Landsat-8 OLI data and the interpreted lithologic map. (A) G. Dara (NED), (B) G. Meatiq (CED), (C) G. Abu Dahr (SED). Note: Gm: gneisses and migmatites; Mu: Metaultramafics; Mg: Metagabbros; Am: Arc metavolcanics; Vom: Volcanogenic metasediments; Og: Older granites; Gd: Gabbro-diorite complex; Dv: Dokhan volcanics; and Yg: Younger granites. The color code of the interpreted maps is shown in Figure 6a and the locations of these selected areas are shown in Figure 4a.

- Abd El-Wahed, M. A. (2010). The Role of the Najd Fault System in the Tectonic Evolution of the Hammamat Molasse Sediments, Eastern Desert, Egypt. *Arab. J. Geosci.* 3, 1–26. doi:10.1007/s12517-008-0030-0
- Abdeen, M. M., and Greiling, R. O. (2005). A Quantitative Structural Study of Late Pan-African Compressional Deformation in the Central Eastern Desert (Egypt) during Gondwana Assembly. *Gondwana Res.* 8 (4), 457–471. doi:10.1016/s1342-937x(05)71148-5
- Abdel Khalek, M. L., Takla, M. A., Sehimi, A., Hamimi, Z., and El Manawi, A. W. (1992). “Geology and Tectonic Evolution of Wadi Beitan Area, South Eastern Desert, Egypt,” in *GAW* (Giza, Egypt: Cairo University), 1, 369–393.

- Abdel-Karim, A. M., and Azzaz, S. A. (1995). On the Age Dating of the Dyke Swarms of Southwestern Sinai, Egypt. *Arab. Gulf J. Sci. Res.* 13, 41–53.
- Abdel-Rahman, A.-F. M. (1996). Pan-African Volcanism: Petrology and Geochemistry of the Dokhan Volcanic Suite in the Northern Nubian Shield. *Geol. Mag.* 133, 17–31. doi:10.1017/s0016756800007226
- Abdelmalik, K. W., and Abd-Allah, A. M. A. (2018). Integration of Remote Sensing Technique and Field Data in Geologic Mapping of an Ophiolitic Suture Zone in Western Arabian Shield. *J. Afr. Earth Sci.* 146, 180–190. doi:10.1016/j.jafrearsci.2017.10.006
- Abdelmalik, K. W. (2019). Landsat 8: Utilizing Sensitive Response Bands Concept for Image Processing and Mapping of Basalts. *Egypt. J. Remote Sens. Space Sci.* 23, 263–274. doi:10.1016/j.ejrs.2019.04.004
- Abdelmalik, K. W. (2018). Role of Statistical Remote Sensing for Inland Water Quality Parameters Prediction. *Egypt. J. Remote Sens. Space Sci.* 21 (2), 193–200. doi:10.1016/j.ejrs.2016.12.002
- Abouelkhair, H., Abdelhalim, A., Hamimi, Z., and Al-Gabali, M. (2020). Reliability of Using ASTER Data in Lithologic Mapping and Alteration Mineral Detection of the Basement Complex of West Berenice, Southeastern Desert, Egypt. *Arab. J. Geosci.* 13, 287. doi:10.1007/s12517-020-5227-x
- Abu El-Ela, F. F. (1997). Geochemistry of an Island-Arc Plutonic Suite: Wadi Dabr Intrusive Complex, Eastern Desert, Egypt. *J. Afr. Earth Sci.* 24, 473–496. doi:10.1016/s0899-5362(97)00076-6
- Akaad, M. K., and Noweir, A. M. (1980). Geology and Lithostratigraphy of the Arabian Desert Orogenic Belt of Egypt between Latitudes 25° 35' and 26° 30' N. *Bull. Inst. Appl. Geol. (King Abdul Aziz Univ. Jeddah)* 3 (4), 127–135. doi:10.1016/b978-0-08-024481-5.50016-9
- Akaad, M. K., Noweir, A. M., and Kotb, H. (1979). Geology and Petrochemistry of the Granite Association of the Arabian Desert Orogenic Belt of Egypt between 25° 35' and 26° 30'. *Delta J. Sci.* 3, 107–151.
- Ali, K. A., Azer, M. K., Gahlan, H. A., Wilde, S. A., Samuel, M. D., and Stern, R. J. (2010). Age Constraints on the Formation and Emplacement of Neoproterozoic Ophiolites along the Allaqi-Heiani Suture, South Eastern Desert of Egypt. *Gondwana Res.* 18, 583–595. doi:10.1016/j.gr.2010.03.002
- Ali, K. A., Kröner, A., Hegner, E., Wong, J., Li, S.-Q., Gahlan, H. A., et al. (2015). U-pb Zircon Geochronology and Hf-Nd Isotopic Systematics of Wadi Beitan Granitoid Gneisses, South Eastern Desert, Egypt. *Gondwana Res.* 27, 811–824. doi:10.1016/j.gr.2013.11.002
- Ali, K., Andresen, A., Manton, W. I., Stern, R. J., Omar, S. A., and Maurice, A. E. (2012). U-pb Zircon Dating and Sr-Nd-Hf Isotopic Evidence to Support a Juvenile Origin of the ~ 634 Ma El Shalul Granitic Gneiss Dome, Arabian-Nubian Shield. *Geol. Mag.* 149, 783–797. doi:10.1017/s0016756811000975
- Ali, K. A., Wilde, S. A., Stern, R. J., Moghazi, A.-K. M., and Ameen, S. M. M. (2013). HF Isotopic Composition of Single Zircons from Neoproterozoic Arc Volcanics and Post-collisional Granites, Eastern Desert of Egypt: Implications for Crustal Growth and Recycling in the Arabian-Nubian Shield. *Precambrian Res.* 239, 42–55. doi:10.1016/j.precamres.2013.05.007
- Ali, S. O. A., and Pour, B. A. (2014). Lithological Mapping and Hydrothermal Alteration Using Landsat 8 Data: a Case Study in Ariab Mining District, Red Sea Hills, Sudan. *Int. J. Basic Appl. Sci.* 3 (3), 199–208. doi:10.14419/ijbas.v3i3.2821
- Andersen, A., Abu El-Rus, M. A., Myhre, P. I., Boghdady, G. Y., and Corfu, F. (2009). U-pb TIMS Age Constraints on the Evolution of the Neoproterozoic Meatiq Gneiss Dome, Eastern Desert, Egypt. *Int. J. Earth Sci. Geol. Rundsch* 98, 481–497.
- Armijo, R., Lacassin, R., Coudurier-Curveur, A., and Carrizo, D. (2015). Coupled Tectonic Evolution of Andean Orogeny and Global Climate. *Earth-Science Rev.* 143, 1–35. doi:10.1016/j.earscirev.2015.01.005
- Asran, A. M., Emam, A., and El-Fakharani, A. (2017). Geology, Structure, Geochemistry and ASTER-Based Mapping of Neoproterozoic Gebel El-Delhimmi Granites, Central Eastern Desert of Egypt. *Lithos* 282–283, 358–372. doi:10.1016/j.lithos.2017.03.022
- Augland, L. E., Andresen, A., and Boghdady, G. Y. (2012). U-pb ID-TIMS Dating of Igneous and Metaigneous Rocks from the El-Sibai Area: Time Constraints on the Tectonic Evolution of the Central Eastern Desert, Egypt. *Int. J. Earth Sci. Geol. Rundsch* 101, 25–37. doi:10.1007/s00531-011-0653-3
- Ballevre, M., Le Goff, E., and Hebert, R. (2001). The Tectonothermal Evolution of the Cadomian Belt of Northern Brittany, France: a Neoproterozoic Volcanic Arc. *Tectonophysics* 331 (1–2), 19–43. doi:10.1016/s0040-1951(00)00234-1
- Bandres, A., Eguiluz, L., Ibarguchi, J. I., and Palacios, T. (2002). Geodynamic Evolution of a Cadomian Arc Region: the Northern Ossa-Morena Zone, Iberian Massif. *Tectonophysics* 352 (1–2), 105–120. doi:10.1016/s0040-1951(02)00191-9
- Bennett, J. D., and Mosley, P. N. (1987). “Tiered-tectonics and Evolution, Eastern Desert and Sinai, Egypt,” in *Current Research in African Earth Sciences*. Editors G. Matheis and H. Schandelmeyer (Rotterdam: Balkema), 79–82.
- Bentor, Y. K. (1985). The Crustal Evolution of the Arabo-Nubian Massif with Special Reference to the Sinai Peninsula. *Precambrian Res.* 28, 1–74. doi:10.1016/0301-9268(85)90074-9
- Bobyarchik, A. R. (1986). The Eigenvalues of Steady State Flow in Mohr Space. *Tectonophysics* 122, 35–52.
- Bregar, M., Bauernhofer, A., Pelz, K., Kloetzli, U., Fritz, H., and Neumayr, P. (2002). A Late Neoproterozoic Magmatic Core Complex in the Eastern Desert of Egypt: Emplacement of Granitoids in a Wrench-Tectonic Setting. *Precambrian Res.* 118, 59–82. doi:10.1016/s0301-9268(02)00062-1
- Breitkreutz, C., Eliwa, H. A., Khalaf, I. M., El Gameel, K., Buhler, B., Sergeev, S., et al. (2010). Neoproterozoic SHRIMP U-Pb Zircon Ages of Silica-Rich Dokhan Volcanics in the North Eastern Desert, Egypt. *Precambrian Res.* 182, 163–174.
- Canadian, O., Koralay, O. E., Topuz, G., Oberhänsli, R., Fritz, H., Collins, A. S., et al. (2016). Late Neoproterozoic Gabbro Emplacement Followed by Early Cambrian Eclogite-Facies Metamorphism in the Menderes Massif (W. Turkey): Implications on the Final Assembly of Gondwana. *Gondwana Res.* 34, 158–173. doi:10.1016/j.gr.2015.02.015
- Chander, G., Markham, B. L., and Helder, D. L. (2009). Summary of Current Radiometric Calibration Coefficients for Landsat MSS, TM, ETM+, and EO-1 ALI Sensors. *Remote Sens. Environ.* 113 (5), 893–903. doi:10.1016/j.rse.2009.01.007
- Chavez, P., Bauer, B., and Sowers, L. B. (1982). An Automatic Pptimum Kernel-Size Selection Technique for Edge Enhancement. *Remote Sens. Environ.* 12 (1), 23–38. doi:10.1016/0034-4257(82)90005-0
- Chen, X., and Campagna, D. J. (2009). “Remote Sensing of Geology,” in *The SAGE Handbook of Remote Sensing*. Editors T. A. Warner, M. D. Nellis, and G. M. Foody (Thousand Oaks, CA: Sage), 328–340.
- Collins, A. S., Blades, M. L., Merdith, A. S., and Foden, J. D. (2021b). Closure of the Proterozoic Mozambique Ocean Was Instigated by a Late Tonian Plate Reorganization Event. *Commun. Earth Environ.* 2. doi:10.1038/s43247-021-00149-z
- Collins, A. S., Blades, M. L., and Merdith, A. S. (2021a). “The Arabian-Nubian Shield within the Neoproterozoic Plate Tectonic Circuit,” in *The Geology of the Arabian-Nubian Shield*. Editors Z. Hamimi, A. R. Fowler, J. P. Liégeois, A. S. Collins, M. G. Abdelsalam, and M. A. El-Wahed (Cham, Switzerland: Regional Geology Reviews, Springer Nature Switzerland), 195–202. doi:10.1007/978-3-030-72995-0\_8
- De Wall, H., Greiling, R. O., and Fouad Sadek, M. (2001). Post-collisional Shortening in the Late Pan-African Hamisana High Strain Zone, SE Egypt: Field and Magnetic Fabric Evidence. *Precambrian Res.* 107, 179–194. doi:10.1016/s0301-9268(00)00141-8
- El Kalioubi, B., Fowler, A.-R., and Abdelmalik, K. (2020). “The Metamorphism and Deformation of the Basement Complex in Egypt,” in *The Geology of Egypt*. Editors Z. Hamimi, A. El-Barkooky, J. Martínez Frías, H. Fritz, and Y. Abd El-Rahman (Cham, Switzerland: Regional Geology Reviews, Springer Nature Switzerland), 191–251. doi:10.1007/978-3-030-15265-9\_6
- El-Bialy, M. Z., and Omar, M. M. (2015). Spatial Association of Neoproterozoic Continental Arc I-type and Post-collision A-type Granitoids in the Arabian-Nubian Shield: The Wadi Al-Baroud Older and Younger Granites, North Eastern Desert, Egypt. *J. Afr. Earth Sci.* 103, 1–29. doi:10.1016/j.jafrearsci.2014.11.013
- El-Gaby, S., el-Nady, O., and Khudeir, A. (1984). Tectonic Evolution of the Basement Complex in the Central Eastern Desert of Egypt. *Geol. Rundsch.* 73, 1019–1036. doi:10.1007/bf01820886
- El-Gaby, S., and Khudeir, A. A. (1988). Low Pressure Metamorphism in Hammamat Sediments at Um Had Area, Central Eastern Desert, Egypt. *Bull. Fac. Assuit Univ.* 17 (2-F), 51–71.
- El-Gaby, S., Khudier, A. A., and El Taky, M. (1989). “The Dokhan Volcanics of Wadi Queh Area, Central Eastern Desert, Egypt,” in 1st Conf. on Geochem, Alexandria, Egypt, 42–62.
- El-Gaby, S., List, F. K., and Tehrani, R. (1988). “Geology, Evolution and Metallogensis of the Pan-African Belt in Egypt,” in *The Pan-African Belt of*

- NE Africa and Adjacent Areas, *Tectonic Evolution and Economic Aspects*. Editors S. El Gaby and R. Greiling (Braunschweig, Wiesbaden: Vieweg), 17–68.
- El-Sharkawy, M. A., and El-Bayoumi, R. M. (1979). The Ophiolites of Wadi Ghadir Area Eastern Desert, Egypt. *Ann. Geol. Surv. Egypt* 9, 125–135.
- Eliwa, H. A., Kimura, J.-I., and Itaya, T. (2006). Late Neoproterozoic Dokhan Volcanics, North Eastern Desert, Egypt: Geochemistry and Petrogenesis. *Precambrian Res.* 151, 31–52. doi:10.1016/j.precamres.2006.08.005
- Emam, A., Hamimi, Z., El-Fakharani, A., Abdel-Rahman, E., Barreiro, J. G., and Abo-Soliman, M. Y. (2018). Utilization of ASTER and OLI Data for Lithological Mapping of Nugrus-Hafafit Area, South Eastern Desert of Egypt. *Arab. J. Geosci.* 11, 756. doi:10.1007/s12517-018-4106-1
- Fowler, A.-R., and Hamimi, Z. (2021a). A Review and Synthesis of Strain Studies in the Egyptian Nubian Shield: Materials, Methods, Problems and Prospects. *Precambrian Res.* 355, 106072. doi:10.1016/j.precamres.2020.106072
- Fowler, A.-R., and Hamimi, Z. (2021b). “Post-amalgamation Depositional Basins in the Arabian-Nubian Shield: The Hammamat Basins of Egypt,” in *The Geology of the Arabian-Nubian Shield. Regional Geology Reviews*. Editors Z. Hamimi, A. R. Fowler, J. P. Liégeois, A. Collins, M. G. Abdelsalam, and M. Abd El-Wahed (Cham, Switzerland: Regional Geology Reviews, Springer Nature Switzerland), 451–483. doi:10.1007/978-3-030-72995-0\_19
- Fowler, A.-R., and Hamimi, Z. (2020). “Structural and Tectonic Framework of Neoproterozoic Basement of Egypt: from Gneiss Domes to Transpression Belts,” in *The Geology of Egypt. Regional Geology Reviews*. Editors Z. Hamimi, A. El-Barkooky, J. Martínez Frias, H. Fritz, and Y. Abd El-Rahman (Cham, Switzerland: Springer Nature Switzerland), 81–129. doi:10.1007/978-3-030-15265-9\_3
- Fowler, A., and Osman, A. F. (2013). Sedimentation and Inversion History of Three Molasse Basins of the Western Central Eastern Desert of Egypt: Implications for the Tectonic Significance of Hammamat Basins. *Gondwana Res.* 23, 1511–1534. doi:10.1016/j.gr.2012.08.022
- Fowler, A., and Osman, A. F. (2009). The Sha’it-Nugrus Shear Zone Separating Central and South Eastern Deserts, Egypt: A Post-arc Collision Low-Angle Normal Ductile Shear Zone. *J. Afr. Earth Sci.* 53, 16–32. doi:10.1016/j.jafrearsci.2008.07.006
- Fritz, H., Abdelsalam, M., Ali, K. A., Bingen, B., Collins, A. S., Fowler, A. R., et al. (2013). Orogen Styles in the East African Orogen: a Review of the Neoproterozoic to Cambrian Tectonic Evolution. *J. Afr. Earth Sci.* 86, 65–106. doi:10.1016/j.jafrearsci.2013.06.004
- Fritz, H., Dallmeyer, D. R., Wallbrecher, E., Loizenbauer, J., Hoinkes, G., Neumayr, P., et al. (2002). Neoproterozoic Tectonothermal Evolution of the Central Eastern Desert, Egypt: a Slow Velocity Tectonic Process of Core Complex Exhumation. *J. Afr. Earth Sci.* 34, 137–155. doi:10.1016/s0899-5362(02)00014-3
- Fritz, H., Loizenbauer, J., and Wallbrecher, E. (2014). Magmatic and Solid State Structures of the Abu Ziran Pluton: Deciphering Transition from Thrusting to Extension in the Eastern Desert of Egypt. *J. Afr. Earth Sci.* 99, 122–135. doi:10.1016/j.jafrearsci.2013.11.012
- Fritz, H., and Messner, M. (1999). Intramontane Basin Formation during Oblique Convergence in the Eastern Desert of Egypt: Magmatically versus Tectonically Induced Subsidence. *Tectonophysics* 315, 145–162. doi:10.1016/s0040-1951(99)00284-x
- Fritz, H., Wallbrecher, E., Khudeir, A. A., Abu El Ela, F., and Dallmeyer, D. R. (1996). Formation of Neoproterozoic Metamorphic Complex during Oblique Convergence (Eastern Desert, Egypt). *J. Afr. Earth Sci.* 23, 311–329. doi:10.1016/s0899-5362(97)00004-3
- Gabr, S. S., Hassan, S. M., and Sadek, M. F. (2015). Prospecting for New Gold-Bearing Alteration Zones at El-Hoteib Area, South Eastern Desert, Egypt, Using Remote Sensing Data Analysis. *Ore Geol. Rev.* 71, 1–13. doi:10.1016/j.oregeorev.2015.04.021
- Gahlan, H. A., Azer, M. K., and Khalil, A. E. S. (2015). The Neoproterozoic Abu Dahr Ophiolite, South Eastern Desert, Egypt: Petrological Characteristics and Tectonomagmatic Evolution. *Min. Pet.* 109, 611–630. doi:10.1007/s00710-015-0397-z
- Gahlan, H. A. (2006). *Petrological Characteristics of the Mantle Section in the Proterozoic Ophiolites from the Pan-African Belt*. Ph.D. thesis (Kanazawa, Japan: Kanazawa Univ.), 227.
- Greiling, R. O., Abdeen, M. M., Dardir, A. A., El Akhal, H., El Ramly, M. F., El Din Kamal, G. M., et al. (1994). A Structural Synthesis of the Proterozoic Arabian-Nubian Shield in Egypt. *Geol. Rundsch.* 83, 484–501. doi:10.1007/bf01083222
- Gupta, R. P. (2013). *Remote Sensing Geology*. Berlin, Heidelberg: Springer-Verlag, 438.
- Hamimi, Z., Abd El-Wahed, M. A., Gahlan, H. A., and Kamh, S. Z. (2019). “Tectonics of the Eastern Desert of Egypt: Key to Understanding the Neoproterozoic Evolution of the Arabian-Nubian Shield (East African Orogen),” in *Geology of the Arab World-An Overview*. Editors A. Bendaoud, Z. Hamimi, M. Hamoudi, S. Djemai, and B. Zoheir (Berlin, Germany: Springer Geology), 1–81. doi:10.1007/978-3-319-96794-3\_1
- Hamimi, Z., Abd El-Wahed, M. A., Hamimi, Z., El-Barkooky, A., Martínez Frias, J., Fritz, H., et al. (2020). “Suture(s) and Major Shear Zones in the Neoproterozoic Basement of Egypt,” in *The Geology of Egypt. Regional Geology Reviews* (Cham, Switzerland: Springer Nature Switzerland), 153–189. doi:10.1007/978-3-030-15265-9\_5
- Hamimi, Z., Hagag, W., Kamh, S., and El-Araby, A. (2020). Application of Remote-Sensing Techniques in Geological and Structural Mapping of Atalla Shear Zone and Environs, Central Eastern Desert, Egypt. *Arab. J. Geosci.* 13, 414. doi:10.1007/s12517-020-05324-8
- Hassan, M. A., and Hashad, A. H. (1990). “Precambrian of Egypt,” in *The Geology of Egypt*. Editor R. Said (Rotterdam: Balkema), 201–245.
- Hassan, S. M., El kazzaz, Y. A., Taha, M. M. N., and Mohammad, A. T. (2017). Late Neoproterozoic Basement Rocks of Meatiq Area, Central Eastern Desert, Egypt: Petrography and Remote Sensing Characterizations. *J. Afr. Earth Sci.* 131, 14–31. doi:10.1016/j.jafrearsci.2017.04.001
- Hassan, S. M., and Ramadan, T. M. (2014). Mapping of the Late Neoproterozoic Basement Rocks and Detection of the Gold-Bearing Alteration Zones at Abu Marawat-Semna Area, Eastern Desert, Egypt Using Remote Sensing Data. *Arab. J. Geosci.* 8, 4641–4656. doi:10.1007/s12517-014-1562-0
- Hassan, S. M., and Sadek, M. F. (2017). Geological Mapping and Spectral Based Classification of Basement Rocks Using Remote Sensing Data Analysis: The Korbaii-Gerf Nappe Complex, South Eastern Desert, Egypt. *J. Afr. Earth Sci.* 134, 404–418. doi:10.1016/j.jafrearsci.2017.07.006
- Hassan, S. M., Soliman, O. S., and Mahmoud, A. S. (2015). Optimized Data Input for the Support Vector Machine Classifier Using ASTER Data. Case Study: Wadi Atalla Area, Eastern Desert, Egypt. *Carpa. J. Earth Environ. Sci.* 10 (1), 15–26.
- Hermina, M., Klitzsch, E., and List, F. K. (1989). *Stratigraphic Lexicon and Explanatory Notes to the Geological Map of Egypt 1:500,000*. Cairo, Egypt: Conoco Inc.
- Horton, B. K., Fuentes, F., Boll, A., Starck, D., Ramirez, S. G., and Stockli, D. F. (2016). Andean Stratigraphic Record of the Transition from Backarc Extension to Orogenic Shortening: A Case Study from the Northern Neuquén Basin, Argentina. *J. S. Am. Earth Sci.* 71, 17–40. doi:10.1016/j.jsames.2016.06.003
- Hu, X., Garzanti, E., Wang, J., Huang, W., An, W., and Webb, A. (2016). The Timing of India-Asia Collision Onset - Facts, Theories, Controversies. *Earth-Science Rev.* 160, 264–299. doi:10.1016/j.earscirev.2016.07.014
- Huntington, J. F. (1996). The Role of Remote Sensing in Finding Hydrothermal Mineral Deposits on Earth. *Ciba Found. Symp.* 202, 214–215. doi:10.1002/9780470514986.ch12
- Hussein, A. A. A., Ali, M. M., and El Ramly, M. F. (1982). A Proposed New Classification of the Granites of Egypt. *J. Volcanol. Geotherm. Res.* 14, 187–198. doi:10.1016/0377-0273(82)90048-8
- Johnson, P. R., Andresen, A., Collins, A. S., Fowler, A. R., Fritz, H., Ghebreab, W., et al. (2011). Late Cryogenian-Ediacaran History of the Arabian-Nubian Shield: a Review of Depositional, Plutonic, Structural, and Tectonic Events in the Closing Stages of the Northern East African Orogen. *J. Afr. Earth Sci.* 61, 167–232. doi:10.1016/j.jafrearsci.2011.07.003
- Johnson, P. R. (2021). “The Arabian-Nubian Shield, an Introduction: Historic Overview, Concepts, Interpretations, and Future Issues,” in *The Geology of the Arabian-Nubian Shield*. Editors Z. Hamimi, A. R. Fowler, J. P. Liegeois, A. Collins, M. Abdelsalam, and M. Abd El-Wahed (Cham, Switzerland: Regional Geology Reviews book series (RGR), Springer Nature Switzerland), 785. doi:10.1007/978-3-030-72995-0
- Jolliffe, I. T. (1986). *Principal Component Analysis*. Berlin, Germany: Springer-Verlag, 487.
- Jones, R. R., Holdsworth, R. E., McCaffrey, K. J. W., Clegg, P., and Tavarnelli, E. (2005). Scale Dependence, Strain Compatibility and Heterogeneity of Three-Dimensional Deformation during Mountain Building: a Discussion. *J. Struct. Geol.* 27, 1190–1204. doi:10.1016/j.jsg.2005.04.001

- Khalil, A. E., El-Desoky, H. M., and Salem, S. M. (2017). Contribution of Remote Sensing Techniques to the Recognition of Titanite Occurrences at Gabal El-Degheimi Area, Central Eastern Desert, Egypt. *Egypt. J. Remote Sens. Space Sci.* 20, 41–50. doi:10.1016/j.ejrs.2016.08.003
- Khudeir, A. A., and Asran, A. H. (1992). Back-arc Wizr Ophiolites at Wadi Um Gheig District, Eastern Desert, Egypt. *Bull. Fac. Sci. Assiut Univ.* 21, 1–22.
- Li, Y., Wang, C., Dai, J., Xu, G., Hou, Y., and Li, X. (2015). Propagation of the Deformation and Growth of the Tibetan-Himalayan Orogen: A Review. *Earth-Science Rev.* 143, 36–61. doi:10.1016/j.earscirev.2015.01.001
- Liégeois, J. P., and Stern, R. J. (2010). Sr–Nd Isotopes and Geochemistry of Granite–Gneiss Complexes from the Meatiq and Hafafit Domes, Eastern Desert, Egypt: No Evidence for Pre-neoproterozoic Crust. *Int. J. Earth Sci.* 57, 31–40.
- Lillesand, T. M., Kiefer, R. W., and Chipman, J. W. (2004). *Remote Sensing and Image Interpretation*. New York: John Wiley & Sons.
- Linnemann, U., and Romer, R. (2002). The Cadomian Orogeny in Saxo-Thuringia, Germany: Geochemical and Nd–Sr–Pb Isotopic Characterization of Marginal Basins with Constraints to Geotectonic Setting and Provenance. *Tectonophysics* 352 (1–2), 33–64. doi:10.1016/s0040-1951(02)00188-9
- Lundmark, A. M., Andresen, A., Hassan, M. A., Augland, L. E., Boghdady, G. Y., and Boghdady, G. Y. (2012). Repeated Magmatic Pulses in the East African Orogen in the Eastern Desert, Egypt: An Old Idea Supported by New Evidence. *Gondwana Res.* 22, 227–237. doi:10.1016/j.gr.2011.08.017
- Messner, M. (1996). *Basin Analysis of Hammamat Type Molasse Basins, Eastern Desert, Egypt*. Cairo, Egypt: Proc. of the Geol. Surv. Egypt, 125–126.
- Moghazi, A. M. (2003). Geochemistry and Petrogenesis of a High-K Calc-Alkaline Dokhan Volcanic Suite, South Safaga Area, Egypt: The Role of Late Neoproterozoic Crustal Extension. *Precambrian Res.* 125, 161–178. doi:10.1016/s0301-9268(03)00110-4
- Mohammad, A. T., El Kazzaz, Y. A., Hassan, S. M., and Taha, M. M. N. (2019). Neoproterozoic Tectonic Evolution and Exhumation History of Transpressional Shear Zones in the East African Orogen: Implications from Kinematic Analysis of Meatiq Area, Central Eastern Desert of Egypt. *Int. J. Earth Sci. Geol. Rundsch.* 109, 253–279. doi:10.1007/s00531-019-01801-y
- Mohy, H., Basta, F., Saber, S., and El Sobky, A. (2017). Using Landsat 8 and ASTER Data for Lithological Discrimination and Mapping in Wadi Hamad Area, North Eastern Desert, Egypt. *J. Amer. Sci.* 13 (7), 1–13.
- Mohy, H., El-Magd, I. A., Basta, F., and Amasha, A. (2019). Utilization of Full-Polarimetric SAR Data (RADARSAT-2), ASTER and Landsat 8 Data in Geological Mapping of the West Gebal Elba Area, Halayeb District, South Eastern Desert, Egypt. *J. Indian Soc. Remote Sens.* 47, 267–278. doi:10.1007/s12524-018-0923-7
- Mouslopoulou, V., Nicol, A., Little, T. A., and Begg, J. G. (2009). “Palaeoearthquake Surface Rupture in a Transition Zone from Strike-Slip to Oblique-Normal Slip and its Implications to Seismic Hazard, North Island Fault System, New Zealand,” in *Palaeoseismology: Historical and Prehistorical Records of Earthquake Ground Effects for Seismic Hazard Assessment*. Editors K. Reicherter, A. M. Michetti, and P. G. Silva (London: Geological Society, London, Special Publications), 316, 269–292. doi:10.1144/sp316.17
- Moussa, E. M. M., Stern, R. J., Manton, W. I., and Ali, K. A. (2008). SHRIMP Zircon Dating and Sm/Nd Isotopic Investigations of Neoproterozoic Granitoids, Eastern Desert, Egypt. *Precambrian Res.* 160, 341–356. doi:10.1016/j.precamres.2007.08.006
- Mwaniki, M. W., Moeller, M. S., and Schellmann, G. (2015). A Comparison of Landsat 8 (OLI) and Landsat 7 (ETM+) in Mapping Geology and Visualising Lineaments: A Case Study of Central Region Kenya. *Int. Arch. Photogramm. Remote Sens. Spat. Inf. Sci.* XL-7/W3, 897–903. doi:10.5194/isprsarchives-xl-7-w3-897-2015
- NOAA (2016). *World Data Service for Geophysics-Bathymetry and Global Relief Grid Extract. Grid Extract*. Washington, D.C., USA: National Oceanic and Atmospheric Administration, National Centers for Environmental Information. Available at: <http://www.ngdc.noaa.gov/mgg/bathymetry/relief.html>.
- Norris, R. J., Koons, P. O., and Cooper, A. F. (1990). The Obliquely-Convergent Plate Boundary in the South Island of New Zealand: Implication for Ancient Collision Zones. *J. Struct. Geol.* 12 (5/6), 715–725. doi:10.1016/0191-8141(90)90084-c
- Pour, A. B., and Hashim, M. (2015). Integrating PALSAR and ASTER Data for Mineral Deposits Exploration in Tropical Environments: a Case Study from Central Belt, Peninsular Malaysia. *Int. J. Image Data Fusion* 6 (2), 170–188. doi:10.1080/19479832.2014.985619
- Raharimahefa, T., and Kusky, T. M. (2009). Structural and Remote Sensing Analysis of the Betsimisaraka Suture in Northeastern Madagascar. *Gondwana Res.* 15, 14–27. doi:10.1016/j.gr.2008.07.004
- Raharimahefa, T., and Kusky, T. M. (2007). Structural and Remote Sensing Studies of the Southern Betsimisaraka Suture, Madagascar. *Gondwana Res.* 10, 186–197.
- Ressetar, R., and Monrad, J. R. (1983). Chemical Composition and Tectonic Setting of the Dokhan Volcanic Formation, Eastern Desert, Egypt. *J. Afr. Earth Sci.* (1983) 1, 103–112. doi:10.1016/0899-5362(83)90002-7
- Sadek, M. F., Ali-Bik, M. W., and Hassan, S. M. (2015). Late Neoproterozoic Basement Rocks of Kadabora-Suwayqat Area, Central Eastern Desert, Egypt: Geochemical and Remote Sensing Characterization. *Arab. J. Geosci.* 8, 10459–10479. doi:10.1007/s12517-015-1973-6
- Sadek, M. F., and Hassan, S. M. (2009). “Rock Discrimination and Geological Mapping of Basement Rocks at Gabal Gharib Area North Eastern Desert of Egypt with Application of Landsat ETM and Egyptsat-1 Data,” in *Remote Sensing for Environmental Monitoring, GIS Applications, and Geology IX*. Editors U. Michel and D. L. Civco (Berlin: Proc. of SPIE), Vol. 4780). doi:10.1117/12.829752
- Sadek, M. S. (1995). Geology, Geochemistry and Structure of Gabal Muqsim Area and Environs, South Eastern Desert, Egypt. *Forschungszentrum Jülich* 32.
- Safari, M., Maghsoudi, A., and Pour, A. B. (2017). Application of Landsat-8 and ASTER Satellite Remote Sensing Data for Porphyry Copper Exploration: a Case Study from Shahr-E-Babak, Kerman, South of Iran. *Geocarto Int.* 33 (11), 1186–1201. doi:10.1080/10106049.2017.1334834
- Sanderson, D. J., and Marchini, W. R. D. (1984). Transpression. *J. Struct. Geol.* 6, 449–458. doi:10.1016/0191-8141(84)90058-0
- Shalaby, A., Stüwe, K., Fritz, H., and Makroum, F. (2006). The El Mayah Molasse Basin in the Eastern Desert of Egypt. *J. Afr. Earth Sci.* 45, 1–15. doi:10.1016/j.jafrearsci.2006.01.004
- Shalaby, A., Stüwe, K., Makroum, F., Fritz, H., Kebede, T., and Klotzli, U. (2005). The Wadi Mubarak Belt, Eastern Desert of Egypt: a Neoproterozoic Conjugate Shear System in the Arabian?Nubian Shield. *Precambrian Res.* 136, 27–50. doi:10.1016/j.precamres.2004.09.005
- Stern, R. J., Ali, K. A., Ren, M., Jarrar, G. H., Romer, R. L., Leybourne, M. I., et al. (2016). Cadomian (~560 Ma) Crust Buried beneath the Northern Arabian Peninsula: Mineral, Chemical, Geochronological, and Isotopic Constraints from NE Jordan Xenoliths. *Earth Planet. Sci. Lett.* 436, 31–42. doi:10.1016/j.epsl.2015.12.026
- Stern, R. J., Ali, K., Hamimi, Z., El-Barkooky, A., Martínez Frías, J., Fritz, H., et al. (2020). “Crustal Evolution of the Egyptian Precambrian Rocks,” in *The Geology of Egypt. Regional Geology Reviews* (Cham, Switzerland: Springer Nature Switzerland), 131–151. doi:10.1007/978-3-030-15265-9\_4
- Stern, R. J. (1994). Arc Assembly and Continental Collision in the Neoproterozoic East African Orogen: Implications for the Consolidation of Gondwanaland. *Ann. Rev. Earth Planet. Sci.* 22, 315–319. doi:10.1146/annurev.ea.22.050194.001535
- Stern, R. J., Gottfried, D., and Hedge, C. E. (1984). Late Precambrian Rifting and Crustal Evolution in the Northeastern Desert of Egypt. *Geol.* 12, 168–172. doi:10.1130/0091-7613(1984)12<168:lprace>2.0.co;2
- Stern, R. J., and Hedge, C. E. (1985). Geochronologic and Isotopic Constraints on Late Precambrian Crustal Evolution in the Eastern Desert of Egypt. *Am. J. Sci.* 285, 97–127. doi:10.2475/ajs.285.2.97
- Stern, R. J., Johnson, P. R., Kröner, A., and Yibas, B. (2004). “Neoproterozoic Ophiolites of the Arabian-Nubian Shield,” in *Precambrian Ophiolites and Related Rocks*. Editor T. M. Kusky (Amsterdam: Elsevier), 95–128. doi:10.1016/s0166-2635(04)13003-x
- Stern, R. J. (2017). Neoproterozoic Formation and Evolution of Eastern Desert Continental Crust-The Importance of the Infrastructure Superstructure Transition. *J. Afr. Earth Sci.* 146, 15–27. doi:10.1016/j.jafrearsci.2017.01.001
- Stoeser, D. B., and Stacey, J. S. (1988). “Evolution, U-Pb Geochronology, and Isotope Geology of the Pan-African Nabitah Orogenic Belt of the Saudi Arabian Shield,” in *The Pan-African Belt of Northeast African and Adjacent Areas*.

- Editors S. El-Gaby and R. O. Greiling (Braunschweig/Wiesbaden: Friedrich, Viewig and Sohn), 227–288.
- Sultan, M., Arvidson, R. E., Sturchio, N. C., and Guinness, E. A. (1987). Lithologic Mapping in Arid Regions with Landsat Thematic Mapper Data: Meatiq Dome, Egypt. *Geol. Soc. Am. Bull.* 99, 748–762. doi:10.1130/0016-7606(1987)99<748:Imiarw>2.0.co;2
- Teyssier, C., and Tikoff, B. (1999). Fabric Stability in Oblique Convergence and Divergence. *J. Struct. Geol.* 21, 969–974. doi:10.1016/s0191-8141(99)00067-x
- Tikoff, B., and Fossen, H. (1993). Simultaneous Pure and Simple Shear: the Unifying Deformation Matrix. *Tectonophysics* 217, 267–283. doi:10.1016/0040-1951(93)90010-h
- Tikoff, B., and Fossen, H. (1999). Three-dimensional Reference Deformations and Strain Facies. *J. Struct. Geol.* 21, 1497–1512. doi:10.1016/s0191-8141(99)00085-1
- Tikoff, B., and Teyssier, C. (1994). Strain Modeling of Displacement-Field Partitioning in Transpressional Orogens. *J. Struct. Geol.* 16, 1575–1588. doi:10.1016/0191-8141(94)90034-5
- Titus, S. J., Housen, B., and Tikoff, B. (2007). A kinematic model for the Rinconada fault system in central California based on structural analysis of en echelon folds and paleomagnetism. *J. Struct. Geol.* 29 (6), 961–982. doi:10.1016/j.jsg.2007.02.004
- Tyagi, P., and Bhosle, U. (2011). Atmospheric Correction of Remotely Sensed Images in Spatial and Transform Domain. *Int. J. Image Proc.* 5 (5), 564–579.
- US Geological Survey (2016). *Landsat 8 (L8) Data User Handbook*. South Dakota: US, EROS Sioux Falls. Version 0.2, 29 March 2016.
- Vincent, R. K. (1997). *Fundamentals of Geological and Environmental Remote Sensing*. Upper Saddle River, NJ: Prentice-Hall, 366–470.
- Willis, K. M., Stern, R. J., and Clauer, N. (1988). Age and Geochemistry of Late Precambrian Sediments of the Hammamat Series from the Northeastern Desert of Egypt. *Precambrian Res.* 42, 173–187. doi:10.1016/0301-9268(88)90016-2
- Xiong, Y., Khan, S. D., Mahmood, K., and Sisson, V. B. (2011). Lithological Mapping of Bela Ophiolite with Remote-Sensing Data. *Int. J. Remote Sens.* 32 (16), 4641–4658. doi:10.1080/01431161.2010.489069
- Xu, Z., Ji, S., Cai, Z., Zeng, L., Geng, Q., and Cao, H. (2012). Kinematics and Dynamics of the Namche Barwa Syntaxis, Eastern Himalaya: Constraints from Deformation, Fabrics and Geochronology. *Gondwana Res.* 21 (1), 19–36. doi:10.1016/j.gr.2011.06.010
- Zimmer, M., Kröner, A., Jochum, K. P., Reischmann, T., and Todt, W. (1995). The Gabal Gerf Complex: a Precambrian N-MORB Ophiolite in the Nubian Shield, NE Africa. *Chem. Geol.* 123, 29–51. doi:10.1016/0009-2541(95)00018-h
- Zoheir, B., El-Wahed, M. A., Pour, A. B., and Abdelnasser, A. (2019a). Orogenic Gold in Transpression and Transtension Zones: Field and Remote Sensing Studies of the Barramiya-Mueilha Sector, Egypt. *Remote Sens.* 11 (2122), 2122. doi:10.3390/rs11182122
- Zoheir, B., Emam, A., Abd El-Wahed, M., and Soliman, N. (2019b). Gold Endowment in the Evolution of the Allaqi-Heiani Suture, Egypt: A Synthesis of Geological, Structural, and Space-Borne Imagery Data. *Ore Geol. Rev.* 110, 102938. doi:10.1016/j.oregeorev.2019.102938
- Zoheir, B., and Emam, A. (2012). Integrating Geologic and Satellite Imagery Data for High-Resolution Mapping and Gold Exploration Targets in the South Eastern Desert, Egypt. *J. Afr. Earth Sci.* 66-67, 22–34. doi:10.1016/j.jafrearsci.2012.02.007

**Conflict of Interest:** The authors declare that the research was conducted in the absence of any commercial or financial relationships that could be construed as a potential conflict of interest.

**Publisher's Note:** All claims expressed in this article are solely those of the authors and do not necessarily represent those of their affiliated organizations, or those of the publisher, the editors, and the reviewers. Any product that may be evaluated in this article, or claim that may be made by its manufacturer, is not guaranteed or endorsed by the publisher.

Copyright © 2022 Hamimi, Hagag, Fritz, Baggazi and Kamh. This is an open-access article distributed under the terms of the Creative Commons Attribution License (CC BY). The use, distribution or reproduction in other forums is permitted, provided the original author(s) and the copyright owner(s) are credited and that the original publication in this journal is cited, in accordance with accepted academic practice. No use, distribution or reproduction is permitted which does not comply with these terms.